arXiv:2603.08511v1 [stat.ME] 9 Mar 2026

# Kantorovich Regression Analysis of Random Distributions with Mixed Predictors

Kaheon Kim[1] and Changbo Zhu*[1]

[1]University of Notre Dame, Department of ACMS

**Abstract**

We study regression problems with distribution-valued responses and mixed distributional and Euclidean predictors. In quadratic cost, the negative gradient of the Kantorovich potential represents, at each source location, the displacement to its matched location under the optimal transport map. By constructing potentials from the Wasserstein barycenter to individual distributions, the proposed Kantorovich regression model approximates the response displacement field as a sum of predictor displacement fields, each adjusted by a functional parameter. Owing to the linear structure, Euclidean predictors can enter as scaling coefficients of $c$-concave parameter potentials. We characterize functional parameter classes ensuring intrinsicness of the model, establish asymptotic theory through uniform convergence of the empirical Wasserstein loss, and derive Gâteaux derivatives leading to first-order optimization algorithms. Real data applications include a mixed-predictor analysis of housing price distributions and an analysis of two-dimensional temperature distributions, demonstrating the flexibility and interpretability of the proposed framework.

**Keywords:** regression analysis, distribution-valued data, optimal transport.

*Zhu's research was supported by NSF DMS-2412832.

## 1. Introduction

Distributions arise naturally in many scientific disciplines as fundamental objects for summarizing information. Rather than reducing observations to a few summary statistics such as the mean or selected quantiles, probability distributions provide a comprehensive description of variability, asymmetry, tail behavior, and multimodality. When each observational unit is associated with a probability distribution, this naturally leads to the analysis of distribution-valued data, where each distribution is treated as a single data point. Examples include age-at-death distributions at the country level [Jdanov et al., 2021], yearly temperature distributions [Bhatia and Katz, 2021], individual-level distributional profiles of physical activity [Matabuena and Petersen, 2023], and subject-specific density estimates for intra-hub brain connectivity [Petersen and Müller, 2016], among others.

Optimal transport has emerged as a geometrically interpretable framework for analyzing distribution-valued data [Panaretos and Zemel, 2016, 2020; Petersen and Müller, 2019; Zhang and Müller, 2011]. Its geometric nature stems from the fact that the optimal transport map moves mass from one distribution to another in the most efficient way, minimizing the total cost of transportation among all mass-preserving maps. Under quadratic cost, the optimal transport map $T$ from a source distribution to a target distribution induces a vector field defined by $x \mapsto T(x) - x$, which we refer to as the displacement field. The Wasserstein barycenter, as a notion of average for distributions [Agueh and Carlier, 2011], satisfies that the average displacement fields from the barycenter to the sample distributions vanish, paralleling the role of the mean in linear spaces. Unlike pointwise averaging of densities, which can produce artificial multimodality when distributions differ mainly by shifts, the Wasserstein barycenter preserves the overall geometric structure of the distributions by aligning and aggregating the transport displacements rather than mixing density values at fixed locations.

In this paper, we study the regression problem where the response is distribution-valued, and the predictors can be distributions, vectors, or both, within the optimal transport framework. By leveraging the displacement structure encoded by Kantorovich potentials relative to Wasserstein barycenters, we develop a regression framework, termed Kantorovich regres-

sion, that models how predictor-induced displacement fields combine to explain variation in the response displacement field. To incorporate distributional predictors, the key mechanism is to scale each predictor displacement field through a one-dimensional functional parameter over the level sets of the corresponding potential function. Equivalently, the Kantorovich potential is deformed by composition with a one-dimensional functional parameter. This can be achieved by composite a smooth function with the Kantorovich potential. This mechanism allows more flexibility than existing approaches that use scalar coefficients and focus primarily on one-dimensional distributions [X. Chen et al., 2024; Zhu and Müller, 2023, 2025]. We then sum the scaled displacement fields and adjust the result by subtracting an intercept term to approximate the response displacement field.

Our design of the scaling operation is motivated by two considerations. First, it ensures intrinsic structure under some regularity conditions: the optimal transport map is cyclically monotone, and to ensure that the predicted transport map preserves this property, Lemma 3.1 shows that the scaling function must remain constant on each connected component of the level sets of the potential function. Determining the connected components of the level sets of a potential function is generally difficult, particularly in multivariate settings, thus a natural choice is to impose uniform scaling over each level set. Methods that utilize the manifold structure of Wasserstein space [Y. Chen et al., 2023], or more generally map distributions to a Hilbert space [Kokoszka et al., 2019; Petersen and Müller, 2016], are considered extrinsic. Second, it provides computational advantages: the scaling parameter is always one-dimensional regardless of the dimensionality of the distributions. We estimate the model parameters by minimizing the Wasserstein loss using first-order gradient descent algorithms, where the distributions and parameter functions are discretized over a regular grid for numerical computation.

For Euclidean predictors, we model each predictor as a uniform scaling factor applied to a parameter displacement field, defined as the gradient of a $c$-concave potential function. The scaled displacement fields from distributional predictors and the parameter displacement fields scaled by Euclidean predictors are summed, and the resulting field is then adjusted by an intercept term to approximate the response displacement field. Another line of approaches, originally proposed by Ghodrati and Panaretos, 2022 and later extended by Y.

Chen et al., 2026; Ghodrati and Panaretos, 2024, focuses on one-dimensional distributions by learning parametric transport maps. It remains unclear how to extend this framework to the mixed predictor setting. Although Girshfeld and Chen, 2025 experimented with multivariate distributions, the approach becomes substantially more computationally challenging. As in multivariate settings, optimal transport maps are vector-valued, making discretization-based algorithms infeasible [Kim et al., 2025, 2026] and typically requiring neural-network-based parameterizations [Girshfeld and Chen, 2025].

The functional model parameters are estimated by minimizing the empirical Wasserstein loss. Building on recent advances in algorithms for optimal transport and Wasserstein barycenter computation [Jacobs et al., 2021; Kim et al., 2025, 2026], we develop first-order gradient-based methods for minimizing the Wasserstein objective. In particular, we derive the Gâteaux derivative of the loss and compute the corresponding gradients. A key technical challenge arises because the functional parameters scale displacement fields over level sets of potential functions, meaning that the parameters are defined on the image of the potentials. Consequently, the gradient of the loss with respect to these parameters is nontrivial to compute, even in the one-dimensional setting. For numerical implementation, the distributions and functions are discretized on regular grids, following the discretization-based computational framework in [Jacobs et al., 2021; Kim et al., 2025, 2026]. For one-dimensional distributions, the resulting objective function is convex, and standard algorithmic guarantees for first-order optimization algorithms apply.

We establish the statistical convergence of the empirical Wasserstein loss to its population counterpart as the sample size tends to infinity under the uniform metric. Our theoretical results rely on standard regularity conditions on the observed Kantorovich potentials $\{\phi_i\}$, such as smoothness or strong convexity of $|x|^2/2 - \phi_i$. Similar conditions are commonly imposed in the optimal transport literature for computational algorithms [Kim et al., 2025; Paty et al., 2020] as well as statistical convergence properties [Chewi et al., 2025; Divol et al., 2025; Hütter and Rigollet, 2021; Manole et al., 2024], among others. For one-dimensional distributions, the population loss function is convex, allowing us to apply $M$-estimation theory to establish consistency of the estimated functional parameters under a separation condition for the true minimizer [Van der Vaart and Wellner, 2023]. For multivariate distributions,

however, the population loss becomes non-convex, and we instead establish convergence of the estimators in terms of excess risk.

We organize the paper as follows. Section 2 introduces basic concepts in optimal transport and Wasserstein barycenters, along with their computational algorithms. Section 3 presents the main methodological developments for Kantorovich regression, starting with a single distributional predictor and extending to mixed predictors. Asymptotic results on the convergence of the estimated model parameters are provided in Section 4. Computational algorithms based on discretization are discussed in Section 5. Numerical experiments on one- and two-dimensional distributions are presented in Section 6. Concluding remarks are given in Section 7. Proofs and additional technical details are collected in the Appendix.

## 2. Preliminary

Throughout the manuscript, let $\Omega \subset \mathbb{R}^d$ be a compact set. For $x, y \in \Omega$, let $\langle x, y\rangle = x^\top y$ denote the Euclidean inner product, and $\|x\| = \sqrt{\langle x, x\rangle}$ the induced Euclidean norm on $\mathbb{R}^d$. The diameter of $\Omega$ is defined as $\mathrm{diam}(\Omega) := \sup_{x,y\in\Omega} \|x - y\| < \infty$. We write $\mathcal{C}^k(\Omega)$ for the space of real-valued functions $\phi : \Omega \to \mathbb{R}$ whose partial derivatives up to order $k$ exist and are continuous on $\Omega$, and use $\nabla\phi(x), \nabla^2\phi(x)$ to represent its gradient vector and hessian matrix at $x$ respectively. For symmetric matrices $A, B \in \mathbb{R}^{d\times d}$, $A \preceq B$ means that $B - A$ is positive semidefinite (PSD). A function $\phi \in \mathcal{C}^1(\Omega)$ is $\alpha$-strongly convex if, for all $x, y \in \Omega$, $\phi(y) \geq \phi(x) + \langle\nabla\phi(x), y - x\rangle + \frac{\alpha}{2}\|y - x\|^2$. If $\phi \in \mathcal{C}^2(\Omega)$, this is equivalent to the uniform Hessian bound $\nabla^2\phi(x) \succeq \alpha I_d$ for all $x \in \Omega$, where $I_d$ is the $d \times d$ identity matrix. A function $\phi \in \mathcal{C}^1(\Omega)$ is $\beta$-smooth if $\phi(y) \leq \phi(x) + \langle\nabla\phi(x), y - x\rangle + \frac{\beta}{2}\|y - x\|^2 \,\forall\, x, y \in \Omega$, and, if $\phi \in \mathcal{C}^2(\Omega)$, this is equivalent to $\nabla^2\phi(x) \preceq \beta I_d$ for all $x \in \Omega$.

### 2.1. Optimal transport

We let $\mathcal{P}_{\mathrm{ac}}(\Omega)$ be the set of absolutely continuous probability measures on $\Omega$. For $\mu \in \mathcal{P}_{\mathrm{ac}}(\Omega)$, its support is denoted as $\mathrm{sp}(\mu)$. For any cost function $c : \Omega \times \Omega \to \mathbb{R}_+$, the $c$-transform of a function $\phi : \Omega \to \mathbb{R}$ is defined as

$$\phi^c(y) = \inf_{x\in\Omega}\{c(x, y) - \phi(x)\}.$$

In this manuscript, we focus on the quadratic cost $c(x, y) = \|x - y\|^2/2$. Letting $T_{\#}\mu$ denote the pushforward measure of $\mu$ by $T : \Omega \to \Omega$, the Monge transportation problem is formulated as

$$\inf_{T:\, T_{\#}\mu=\nu} \int_{\Omega} c(T(x), x)\, \mathrm{d}\mu(x), \qquad \text{(MP)} \tag{1}$$

where the minimization is over the set of maps $T : \Omega \to \Omega$ such that $T_{\#}\mu = \nu$. If $\mu, \nu \in \mathcal{P}_{\mathrm{ac}}(\Omega)$, the solution $T$ to the Monge problem is $\mu$-a.e. unique. This map is called the *optimal transport map* from $\mu$ to $\nu$, and is denoted by $T_{\mu\to\nu}$. In this case, the quadratic Wasserstein distance between $\mu$ and $\nu$ is $W_2(\mu, \nu) := 2\left(\int_{\Omega} c\big(T_{\mu\to\nu}(x), x\big)\, \mathrm{d}\mu(x)\right)^{1/2}$. For discrete measures, the Monge problem often has no solution because it does not allow mass to be split in order to match the target weights. In contrast, the Kantorovich (relaxed) formulation always admits a solution, and defines

$$W_2^2(\mu, \nu) := \inf_{\pi\in\Pi(\mu,\nu)} \int_{\Omega\times\Omega} \frac{1}{2}\|x - y\|^2\, \mathrm{d}\pi(x, y),$$

where $\Pi(\mu, \nu)$ denotes the set of all couplings (joint distributions) on $\Omega \times \Omega$ with marginals $\mu$ and $\nu$. A function $\phi : \Omega \to \mathbb{R}$ is called $c$-concave if $\phi = \psi^c$ for some $\psi : \Omega \to \mathbb{R}$. We use $c$-conc$(\Omega)$ to denote the set of $c$-concave functions. The dual of Kantorovich formuation can be written as

$$\sup_{\phi\in c\text{-conc}(\Omega)} \int_{\Omega} \phi\, \mathrm{d}\mu + \int_{\Omega} \phi^c\, \mathrm{d}\nu. \qquad \text{(DP)} \tag{2}$$

For absolutely continuous measures, we have inf (MP) = sup (DP). Any maximizer of (DP) is called a *Kantorovich potential* and is unique $\mu$-a.e. up to an additive constant. In statistical analysis, a unique representative, denoted by $\phi_{\mu\to\nu}$, can be selected by requiring it to satisfy a normalization condition, such as $\int_{\Omega} \phi_{\mu\to\nu}(x)\, \mathrm{d}\mu(x) = 0$. The optimal transport map and the Kantorovich potential satisfy $T_{\mu\to\nu}(x) = x - \nabla\phi_{\mu\to\nu}(x), x \in \Omega$, and this motivates us to define

$$T_{\phi} := \mathrm{id} - \nabla\phi \text{ for any } c\text{-concave } \phi.$$

Moreover, when $\phi$ is $c$-concave, the function $\frac{\|x\|_2^2}{2} - \phi(x)$ is convex (see [Santambrogio, 2015]), which implies that $T_{\mu\to\nu} = \nabla u$ for some convex function $u : \Omega \to \mathbb{R}$. This result is commonly

referred as the Brenier theorem (Brenier, 1991). A map $T : \mathbb{R}^d \to \mathbb{R}^d$ is said to be cyclically monotone if, for any integer $m \geq 2$ and any collection of points $\{x_1, \ldots, x_m\} \subset \mathbb{R}^d$,

$$\sum_{i=1}^{m} \langle T(x_i),\, x_i - x_{i+1} \rangle \geq 0, \qquad x_{m+1} := x_1.$$

A classical result of Rockafellar [Rockafellar, 1966] states that $T$ is cyclically monotone if and only if there exists a proper, lower semicontinuous convex function $\varphi : \mathbb{R}^d \to \mathbb{R} \cup \{+\infty\}$ such that $T(x) \in \partial\varphi(x)$ for all $x \in \mathbb{R}^d$, where $\partial\varphi$ denotes the subdifferential of $\varphi$. This implies that $T_{\mu\to\nu}$ between absolutely continuous $\mu$ and $\nu$ is cyclically monotone.

In a metric space $(\mathcal{M}, d)$, a geodesic is a constant-speed curve $\gamma : [0,1] \to \mathcal{M}$ such that $d(\gamma(s), \gamma(t)) = |t - s|\, d(\gamma(0), \gamma(1))$ for all $s, t \in [0,1]$. $(\mathcal{P}_{\mathrm{ac}}(\Omega), W_2)$ is a metric space and for any $\mu_1, \mu_2 \in \mathcal{P}_{\mathrm{ac}}(\Omega)$, the geodesic $\gamma_{\mu_1,\mu_2}$ connecting them is given by $\gamma_{\mu_1,\mu_2}(t) := ((1-t)\,\mathrm{id} + tT_{\mu_1\to\mu_2})_{\#}\mu_1$. A functional $F : \mathcal{P}_{\mathrm{ac}}(\Omega) \to \mathbb{R}$ is said to be geodesically convex if $F(\gamma_{\mu_1,\mu_2}(t)) \leq (1-t)F(\mu_1) + tF(\mu_2)$ for any $\mu_1, \mu_2 \in \mathcal{P}_{\mathrm{ac}}(\Omega)$ and any $t \in [0,1]$.

### 2.2. Wasserstein barycenter

Let $P_\mu$ be a probability measure on $\mathcal{P}_{\mathrm{ac}}(\Omega)$, and let $\mu \sim P_\mu$ denote a random measure drawn from it. The (population) Wasserstein barycenter of $P_\mu$, denoted $\bar{\mu}$, is defined as the unique minimizer of the barycenter functional $B : \mathcal{P}_{\mathrm{ac}}(\Omega) \to \mathbb{R}$, where

$$B(\omega) := \int_{\mathcal{P}_{\mathrm{ac}}(\Omega)} W_2^2(\omega, \mu')\, \mathrm{d}P_\mu(\mu').$$

Given i.i.d. samples $\mu_1, \ldots, \mu_n \sim P_\mu$, the empirical Wasserstein barycenter $\bar{\mu}_n$ is the unique minimizer of $\widehat{B}(\omega) := \frac{1}{n}\sum_{i=1}^{n} W_2^2(\omega, \mu_i)$.

Below, we discuss first-order gradient-based algorithms for minimizing $\widehat{B}$. This discussion will be useful for designing computational algorithms for learning the parameters of the proposed Kantorovich regression model. We first review the basic notions of gradients in Hilbert spaces and in Wasserstein space, which will be instrumental for optimizing the proposed model. Gâteaux derivative generalizes the standard notion of a directional derivative to functionals. Given a Hilbert space $\mathcal{H}$ with inner product $\langle \cdot, \cdot \rangle_{\mathcal{H}}$, the Gâteaux derivative of a functional $G : \mathcal{H} \to \mathbb{R}$ at a point $g \in \mathcal{H}$ in the direction $h \in \mathcal{H}$, denoted by $\delta G_g(h)$, is

defined as

$$\delta G_g(h) = \frac{\mathrm{d}}{\mathrm{d}\epsilon} G(g + \epsilon h)\bigg|_{\epsilon=0}.$$

If for all $g, h \in \mathcal{H}$, we can express $\delta G_g(h) = \langle \boldsymbol{\nabla} G(g), h \rangle_{\mathcal{H}}$ for some map $\boldsymbol{\nabla} G : \mathcal{H} \to \mathcal{H}$, the $\mathcal{H}$-gradient of $G$ is then defined to be $\boldsymbol{\nabla} G$. When $\mathcal{H}$ is $\mathbb{R}^d$, $\boldsymbol{\nabla} G$ simplifies to the standard gradient of a function. On the other hand, let $H : \mathcal{P}_{\mathrm{ac}}(\Omega) \to \mathbb{R}$ be a functional admitting a first variation $\frac{\delta H}{\delta \mu}(\mu) : \Omega \to \mathbb{R}$, which identified up to an additive constant by

$$\frac{\mathrm{d}}{\mathrm{d}\varepsilon}\bigg|_{\varepsilon=0} H((1-\varepsilon)\mu + \varepsilon\nu) = \int_\Omega \frac{\delta H}{\delta \mu}(\mu)\, \mathrm{d}(\nu - \mu),$$

for all $\nu \in \mathcal{P}_{\mathrm{ac}}(\Omega)$ for which the derivative exists. The Wasserstein gradient of $H$ at $\mu$ is defined as $\mathbb{\nabla} H(\mu) := \nabla \frac{\delta H}{\delta \mu}(\mu)$.

By expanding the Wasserstein distance with the Kantorovich dual form, Kim et al., 2025 propose to formulate barycenter problem as a minimax optimization problem

$$\min_{\omega \in \mathcal{P}_{\mathrm{ac}}(\Omega)} \sup_{\phi_1, \ldots, \phi_n} J(\omega, \phi_1, \ldots, \phi_n) := \frac{1}{n} \sum_{i=1}^n \int_\Omega \phi_i \, \mathrm{d}\omega + \int_\Omega \phi_i^c \, \mathrm{d}\mu_i.$$

The functional $J$ is not geodesically convex in $\omega$ but is concave in each $\phi_i$, and therefore gives rise to a nonconvex–concave optimization problem. To address this structure, Kim et al., 2025 proposed a Wasserstein-descent $\dot{\mathcal{H}}^1$-ascent algorithm utilizing the Wasserstein gradient and $\dot{\mathcal{H}}^1$-gradient for each component, where $\dot{\mathcal{H}}^1$ denotes a homogeneous Sobolev space. On the other hand, Kim et al., 2026 showed that the barycenter problem can be reformulated as a purely concave optimization problem and proposed a $\dot{\mathcal{H}}^1$-ascent algorithm for its solution. Owing to this simplified structure, they were able to establish explicit convergence guarantees for the algorithm. We refer the reader to (Kim et al., 2025) and (Kim et al., 2026) for full implementation and computational details of the two approaches.

## 3. Kantorovich Regression

Given two distributions $\mu_1, \mu_2 \in \mathcal{P}_{\mathrm{ac}}(\Omega)$, we recall that the gradient of the Kantorovich potential $\nabla \phi_{\mu_1 \to \mu_2}$ and the optimal transport $T_{\mu_1 \to \mu_2}$ are connected through

$$-\nabla \phi_{\mu_1 \to \mu_2}(x) \;=\; T_{\mu_1 \to \mu_2}(x) - x,$$

so $-\nabla\phi_{\mu_1\to\mu_2}(x)$ is the displacement vector from each location $x$ in the source distribution to its optimally matched location in the target distribution. In addition, if $\bar{\mu}$ denotes the Wasserstein barycenter of a random distribution $\mu$, then the average displacement at each $x$ satisfies

$$\mathrm{E}_\mu[\nabla\phi_{\bar{\mu}\to\mu}(x)] = 0.$$

The barycenter serves as the mean of $\mu$, and the displacement field $\nabla\phi_{\bar{\mu}\to\mu}$ encodes how $\mu$ departs from $\bar{\mu}$, which directly parallels the Euclidean case $\mathrm{E}[X - \mathrm{E}[X]] = 0$ for any random vector $X \in \mathbb{R}^d$. In the ordinary regression model $Y - \mathrm{E}[Y] = A(X - \mathrm{E}[X]) + \epsilon$, multiplying by the model parameters $A \in \mathbb{R}^{d\times d}$ can be interpreted as an adjustment step for the displacement vector $X - \mathrm{E}[X]$. If $A$ is a scalar, then the adjustment is uniform across all entries of $X - \mathrm{E}[X]$. Since $-\nabla\phi_{\bar{\mu}\to\mu}(x)$ and $\nabla\phi_{\bar{\mu}\to\mu}(x)$ differ only by a sign, which does not affect the modeling framework, we henceforth focus on $\nabla\phi_{\bar{\mu}\to\mu}(x)$ for convenience.

Motivated by the analogies, we construct our regression model by first proposing an non-uniform adjustment of the displacement field $\nabla\phi_{\bar{\mu}\to\mu}$. In particular, given a function $f \in C^2(\mathbb{R})$ and a $c$-concave potential $\phi : \Omega \to \mathbb{R}$, we define

$$f \circledcirc \phi := \begin{cases} f \circ \phi, & \text{if } f \text{ is non-decreasing and concave;} \\ -f \circ (-\phi), & \text{if } f \text{ is non-increasing and convex.} \end{cases} \tag{3}$$

The function $f$ can be seen as the functional parameter, and by applying this operation on $\phi_{\bar{\mu}\to\mu}$, the adjusted displacement at $x$ becomes

$$\nabla(f \circledcirc \phi_{\bar{\mu}\to\mu})(x) = \begin{cases} f'(\phi_{\bar{\mu}\to\mu}(x))\,\nabla\phi_{\bar{\mu}\to\mu}(x) & \text{if } f \text{ is non-decreasing and concave.} \\ f'(-\phi_{\bar{\mu}\to\mu}(x))\nabla\phi_{\bar{\mu}\to\mu}(x) & \text{if } f \text{ is non-increasing and convex.} \end{cases}$$

When $f$ is non-decreasing and concave, the displacement direction remains $\nabla\phi_{\bar{\mu}\to\mu}(x)$, while the length is rescaled by $f'(\phi_{\bar{\mu}\to\mu}(x)) \geq 0$. Points sharing the same level set $\{x : \phi_{\bar{\mu}\to\mu}(x) = a\}$ receive identical scaling $f'(a)$, and the scaling varies across level sets. When $f$ is non-increasing and convex, $-f'(-\phi_{\bar{\mu}\to\mu}(x)) \geq 0$. The direction becomes opposite to $\nabla\phi_{\bar{\mu}\to\mu}(x)$ and its magnitude is rescaled by $-f'(-\phi_{\bar{\mu}\to\mu}(x))$. Again, points sharing a level set $\{x : -\phi_{\bar{\mu}\to\mu}(x) = b\}$ receive the same non-positive multiplier $-f'(b)$ and the scaling varies from one level set to the next. When $f(t) = at$ for some fixed $a \in \mathbb{R}$, $f \circledcirc \phi = a\phi$ regardless of

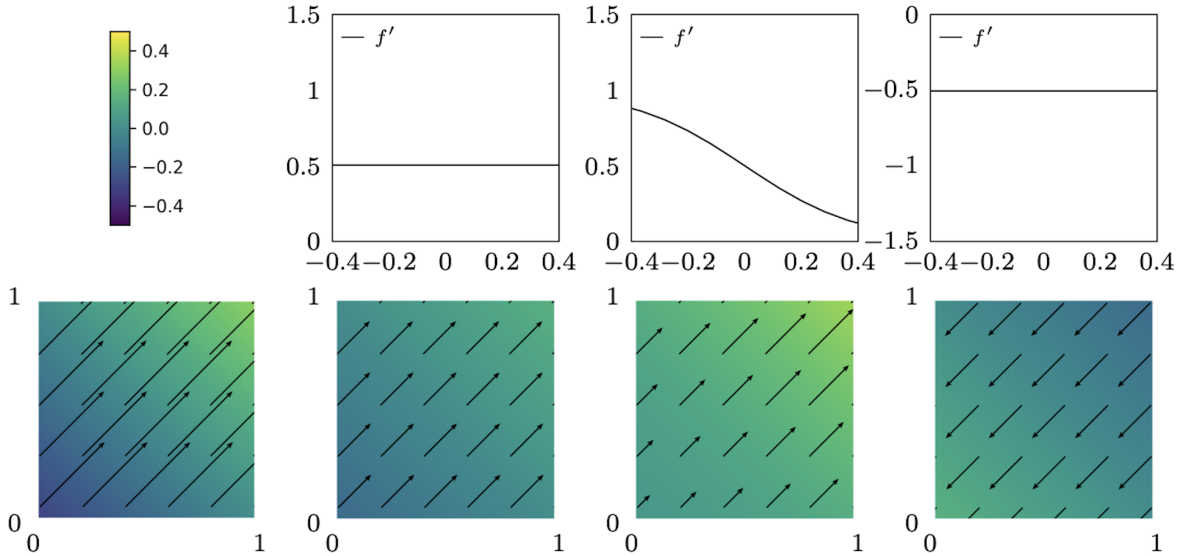


Figure 1: Illustration of the adjustment on $\phi$ by $f$. Column 1 (bottom row) shows the Kantorovich potential $\phi : [0,1]^2 \to \mathbb{R}$ as a heat map, together with the gradient field $\nabla\phi$ drawn as arrows. From column 2 onward, the top row displays the derivatives $f'$ of the functional parameter $f$, while the bottom row shows $f \circledcirc \phi$ as heat maps with the corresponding gradient field $\nabla(f \circledcirc \phi)$ (arrows).

the sign of $a$ and this adjustment of displacement vector $\nabla\phi(x)$ by $f$ is uniform in $x$. Figure 1 illustrates how the function $f$ adjusts a two-dimensional potential $\phi$ and its corresponding displacement field.

We recall that valid optimal transport maps are cyclically monotone. The lemma below states that suppose one attempts to modify the displacement field by replacing $\nabla\phi(x)$ with $g(x)\,\nabla\phi(x)$ for some function $g : \Omega \to \mathbb{R}$. In order for the resulting map $x \mapsto x - g(x)\,\nabla\phi(x)$ to remain cyclically monotone, the function $g$ must be constant on each connected component of every level set of $\phi$. Since identifying the connected components of the level sets of a potential function is generally difficult, adjustments of the form $T_{f\circ\phi}(x) := x - f'(\phi(x))\nabla\phi(x)$ provide a natural and convenient way to construct feasible modifications of transport maps.

**Lemma 3.1.** *Given a c-concave function $\phi \in \mathcal{C}^2(\Omega)$ such that $\nabla\phi(x) \neq 0$ for any $x \in \Omega$ and $g \in \mathcal{C}^1(\mathbb{R})$, we let $R(x) := x - g(x)\nabla\phi(x)$. If $R$ is cyclically monotone, then $g$ is constant on each connected component of each level set $S_a = \{x : \phi(x) = a\}$.*

### 3.1. Single distributional predictor

We first consider regression of the distributional response on a single distributional predictor. Let $P_{\nu,\mu}$ be a joint distribution on $\mathcal{P}_{\mathrm{ac}}(\Omega) \times \mathcal{P}_{\mathrm{ac}}(\Omega)$, $(\nu, \mu) \sim P_{\nu,\mu}$, and $\{(\nu_i, \mu_i)\}_{i=1}^n$ be i.i.d. copies of $(\nu, \mu)$. The marginal distributions on $\nu$ and $\mu$ are denoted as $P_\nu$ and $P_\mu$ respectively, and their population Wasserstein barycenters are $\bar{\nu}$ and $\bar{\mu}$.

In practice, distributions are estimated from finite samples, and their supports are difficult to determine. A convenient and statistically effective approach is to estimate all distributions on a common domain using standard procedures such as kernel density estimation. Typical choices of the common domain include the entire space $\mathbb{R}^d$, a bounded interval $[a, b]$ for one-dimensional distributions, or a rectangle $[a, b] \times [c, d]$ for two-dimensional distributions. In such settings, all distributions involved in the regression analysis share the same support. Motivated by this practice, we consider throughout the paper the case in which the barycenters of the predictor and response distributions have identical support, i.e., $\mathrm{sp}(\bar{\nu}) = \mathrm{sp}(\bar{\mu})$. This setting includes the common support scenario described above as a special case. The handling of situation in which $\mathrm{sp}(\bar{\nu}) \neq \mathrm{sp}(\bar{\mu})$ is discussed separately in Remark 3.4.

The key idea of our Kantorovich regression is to explain variability in the response displacement field $\nabla\phi_{\bar{\nu}\to\nu_i}$ through adjustments of the predictor displacement field $\nabla\phi_{\bar{\mu}\to\mu_i}$ via the operation defined in Equation 3. Incorporating random error via a random cyclically monotone transport map $T_{\varepsilon_i} : \Omega \to \Omega$ such that $\mathrm{E}[T_{\varepsilon_i}] = \mathrm{id}$, the resulting Kantorovich regression (KR) model with a single distributional predictor is given by

$$\nu_i = (T_{\varepsilon_i})_{\#}\left(T_{f\circledcirc\phi_i - \mathrm{E}[f\circledcirc\phi_i]}\right)_{\#}\bar{\nu}, \tag{4}$$

where $\phi_i = \phi_{\bar{\mu}\to\mu_i}$ and $f : \mathbb{R} \to \mathbb{R}$ is the functional parameter that is either non-decreasing and concave or non-increasing and convex. Here, $f \circledcirc \phi_i$ denotes the adjusted potential function, which is further centered by subtracting the intercept term $\mathrm{E}\left[f \circledcirc \phi_i\right]$. When $f(t) = at$ for some $a \in \mathbb{R}$, the operation $f \circledcirc \phi_i$ is linear in $\phi_i$, and the intercept term vanishes, i.e., $\mathrm{E}\left[f \circledcirc \phi_i\right] = 0$. For a general (nonlinear) functional parameter $f$, this centering is necessary to ensure that

$$\mathrm{E}\left[T_{f\circledcirc\phi_i - \mathrm{E}[f\circledcirc\phi_i]}(x)\right] = x,$$

so that the barycenter of the response distributions $\nu_i$ remains $\bar{\nu}$.

For a matrix $A \in \mathbb{R}^{m\times m}$, the operator norm induced by the Euclidean norm is defined as $\|A\|_{\mathrm{op}} := \sup_{\|x\|_2=1} \|Ax\|_2$. Consider the set

$$\mathbb{K}(\gamma_-, \gamma_+) := \Big\{\phi \in \mathcal{C}^2(\Omega) : \int_\Omega \phi \, \mathrm{d}\bar{\nu} = 0 \text{ and } \forall x \in \Omega, a \le \phi(x) \le b, \\ \|\nabla\phi(x)\| \le \mathrm{diam}(\Omega), -\gamma_- I_d \preceq \nabla^2\phi(x) \preceq \gamma_+ I_d\Big\}. \quad (5)$$

$\mathbb{K}(\gamma_-, \gamma_+)$ defines a set of potential functions whose curvatures are uniformly controlled by $\gamma_-$ and $\gamma_+$. We note that any twice differentiable $c$-concave function $\varphi$ is 1-smooth, i.e., $\nabla^2\varphi(x) \preceq I_d$ and thus $\gamma_+ \le 1$. In contrast, the constant $\gamma_-$ may be large. Let

$$\mathbb{F}_+(\kappa_1, \kappa_2) := \{f \in \mathcal{C}^2([a,b]) : 0 \le f'(t) \le \kappa_1,\ -\kappa_2 \le f''(t) \le 0,\ \forall\, t \in [a,b]\}.$$

be a class of non-decreasing concave functional parameters and $\mathbb{F}_-(\kappa_1, \kappa_2) := \{f \in \mathcal{C}^2([a,b]) : 0 \le -f'(t) \le \kappa_1,\ -\kappa_2 \le -f''(t) \le 0,\ \forall\, t \in [a,b]\}$ be the set of non-increasing convex functions. The constants $\kappa_1, \kappa_2$ can be selected, depending on the data-generating distribution $P_{\mu,\nu}$, so that the centered potential $f \circledcirc \phi_i - \mathrm{E}\,[f \circledcirc \phi_i]$ is $c$-concave. Consequently, the associated transport map $T_{f\circledcirc\phi_i - \mathrm{E}[f\circledcirc\phi_i]}$ is cyclically monotone.

**Theorem 3.2.** *Let* $\eta := \sup_{x\in\mathrm{sp}(\bar{\nu})} \mathrm{E}_{\mu_i}[\|\nabla\phi_i(x)\|^2]$ *and* $\lambda := \sup_{x\in\mathrm{sp}(\bar{\nu})}(\mathrm{E}_{\mu_i}[\|\nabla^2\phi_i(x)\|_{\mathrm{op}}^2])^{1/2}$. *Assuming that* $\phi_i \in \mathbb{K}(\gamma_-, \gamma_+)$ *almost surely, then for each* $\delta \in \{+,-\}$, *by choosing* $\kappa_{1,\delta}, \kappa_{2,\delta}$ *to satisfy*

$$(\gamma_\delta + \lambda)\kappa_{1,\delta} + \eta\kappa_{2,\delta} \le 1, \quad (6)$$

*the function* $f \circledcirc \phi_i - \mathrm{E}_{\mu_i}\,[f \circledcirc \phi_i]$ *is c-concave for any* $f \in \bigcup_{\delta\in\{+,-\}} \mathbb{F}_\delta(\kappa_{1,\delta}, \kappa_{2,\delta})$.

If the sign indicator $\delta = +$, we fit a model with a non-decreasing concave functional parameter. If $\delta = -$, we fit a model with a non-increasing convex functional parameter. The constants $\eta, \lambda, \gamma_-, \gamma_+$ depend on the generating distribution $P_{\nu,\mu}$ and can be estimated from data. In particular, $\eta$ represents the maximum displacement on average. Although $\lambda \le \max\{\gamma_-, \gamma_+\}$, the value of $\lambda$ can be substantially smaller, since it is a population-level quantity defined through an expectation. If the optimal transport $T_{\phi_i}$ is linear almost surely, then $\nabla^2\phi_i = 0$. Consequently, we may take $\gamma_- = \gamma_+ = \lambda = 0$, and the constants $\kappa_{1,-}, \kappa_{1,+}$ can be chosen arbitrarily large. Condition 6 can always be made true by selecting $\kappa_{1,+}, \kappa_{2,+}, \kappa_{1,-}, \kappa_{2,-}$ small enough.

When $f(t) = at$, we have $f \circledcirc \phi_i = a\phi_i$ for any $a \in \mathbb{R}$, the intercept term $\mathrm{E}[f \circledcirc \phi_i] = 0$ and model (4) reduces to

$$\nu_i = (T_{\varepsilon_i})_{\#} \left(\mathrm{id} - a\nabla\phi_i\right)_{\#} \bar{\nu}.$$

In this case, we can set $\kappa_{2,+} = \kappa_{2,-} = 0$, and the sufficient conditions in the preceding theorem simplifies accordingly, yielding the following corollary.

**Corollary 3.3.** *Let $f(t) = at$ for some $a \in \mathbb{R}$. If $\phi_i \in \mathbb{K}(\gamma_-, \gamma_+)$ almost surely, then by choosing $\kappa_{1,+}$ and $\kappa_{1,-}$ to satisfy $\kappa_{1,+}\gamma_+ \leq 1$ and $\kappa_{1,-}\gamma_- \leq 1$ respectively, the function $f \circledcirc \phi_i = a\phi_i$ is c-concave for any $-\kappa_{1,-} \leq a \leq \kappa_{1,+}$.*

The functional parameter $f$ is infinite dimensional and, for computational purposes, must be discretized on a fixed grid $a = z_1 < z_2 < \cdots < z_K = b$ that covers the union of the images of $\{\phi_i\}$. When $f$ is non-decreasing and concave, its derivative $f'$ is nonnegative and non-increasing. We can approximate $f'$ using a stepwise function of the form $\sum_{k=1}^{K} \theta_k \mathbf{1}_{\{x \leq z_k\}}$, where $\theta_k \geq 0$ are parameters, and the discretization error can be controlled by refining the grid, that is, by increasing $K$. Furthermore, we let

$$f'_\theta(x) = \sum_{k=1}^{K} \frac{\theta_k}{1 + \exp\big(\theta_0(x - z_k)\big)} \tag{7}$$

be a smooth approximation to the stepwise function $\sum_{k=1}^{K} \theta_k \mathbf{1}_{\{x \leq z_k\}}$. It can be seen that as $\theta_0 \to \infty$, $f'_\theta(x)$ converges to $\sum_{k=1}^{K} \theta_k \mathbf{1}_{\{x \leq z_k\}}$.

We next provide one-dimensional and two-dimensional examples with functional parameter $f_\theta$ that satisfy the assumptions in Theorem 3.2. For a 1D example, we fix $\bar{\mu}$ as normal distribution $N(0.5, 0.1^2)$ truncated on the interval $[0, 1]$, and construct $\mu_i = (T_i)_{\#}\bar{\mu}$ for $i = 1, 2, 3$, where $T_1(x) = \frac{1-e^{-x}}{1-e^{-1}}, T_2(x) = \frac{e^x - 1}{e-1}$ and $T_3(x) = 3x - T_1(x) - T_2(x)$. We set $-0.05 = z_1 < \cdots < z_{100} = 0.05$ that cover the range of the $\phi_{\bar{\mu}\to\mu_i}$ and consider three parameter settings of $\{\theta_k\}$: (1) $\theta_k = 2 \times 10^{-4}\, k$, $\theta_0 = 0$ so that $f_\theta(t) = 0.505\, t$; (2) $\theta_k = 2 \times 10^{-4}\, k$, $\theta_0 = 100$, and it holds that $f_\theta \in \mathbb{F}_+(0.9925, 13.39)$; (3) $\theta_k = 5 \times 10^{-4}\, k$, $\theta_0 = 0$ and $f_\theta(t) = 1.2625\, t$. We then set $\bar{\nu} = \bar{\mu}$, $\varphi_i = f_\theta \circ \phi_{\bar{\mu}\to\mu_i} - \frac{1}{3}\sum_{j=1}^{3} f_\theta \circ \phi_{\bar{\mu}\to\mu_j}$ and $\nu_i = (T_{\varphi_i})_{\#}\bar{\nu}$. These distributions and potential functions are plotted in Figure 2 and 3. It can be computed that $\eta = \frac{(\sqrt{e}-1)^2}{6\,(\sqrt{e}+1)^2} \approx 9.998 \times 10^{-3}$, $\lambda = \frac{1}{\sqrt{3}(e-1)}\sqrt{2e^2 - 10e + 14} \approx 0.4244$, and $\phi_i \in \mathbb{K}(\gamma_-, \gamma_+)$

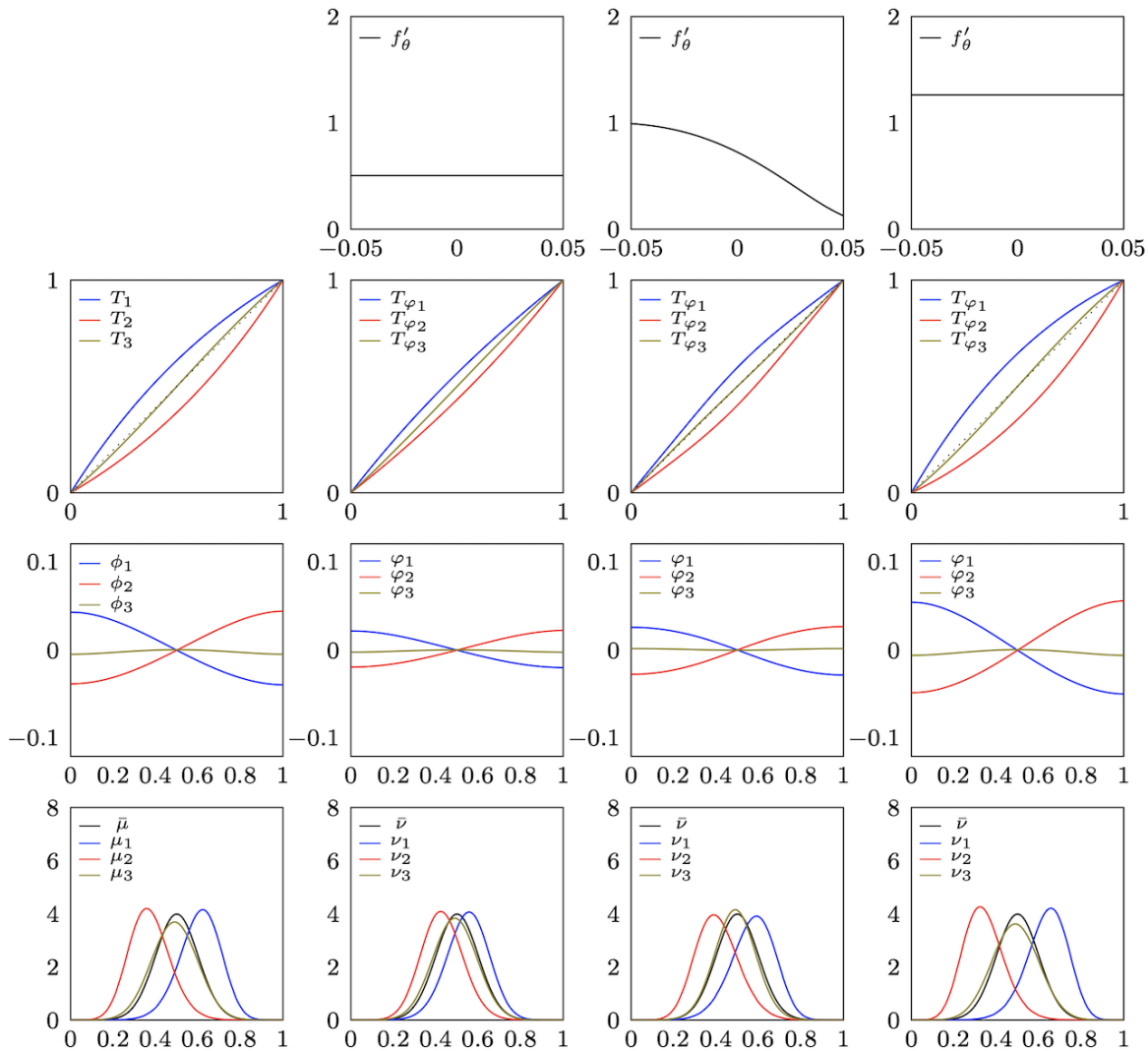


Figure 2: 1D illustration of KR model with non-decreasing concave functional parameter.

with $\gamma_- = \frac{1}{e-1} \approx 0.5820$, $\gamma_+ = \frac{e-2}{e-1} \approx 0.4180$, thus $f_\theta$ under settings (1) and (3) satisfy the condition in Corollary 3.3, and under setting (2) satisfies the condition (6).

From Figure 2, we observe when $f'$ is given as a non-increasing and concave function, the relative locations of $\mu_1, \mu_2, \mu_3$ with respect to $\bar{\mu}$ are preserved in $\nu_1, \nu_2, \nu_3$ with respect to $\bar{\nu}$: $\mu_1$ and $\nu_1$ are on the right, $\mu_2$ and $\nu_2$ are on the left, and $\mu_3$ and $\nu_3$ are in the center. Under setting (1) (second column of Figure 2), $f_\theta(t) = 0.505t$, the distributions $\nu_1$ and $\nu_2$ move closer to $\bar{\nu}$ than $\mu_1$ and $\mu_2$ are to $\bar{\mu}$. Conversely, in the fourth column $f_\theta(t) = 1.2625t$, $\nu_1$ and $\nu_2$ are farther from $\bar{\nu}$ than $\mu_1$ and $\mu_2$ are from $\bar{\mu}$. The third column for setting (2) exhibits the same locational effects as (1). However, $\nu_3$ lies above $\bar{\nu}$ while $\mu_3$ lies below $\bar{\mu}$,

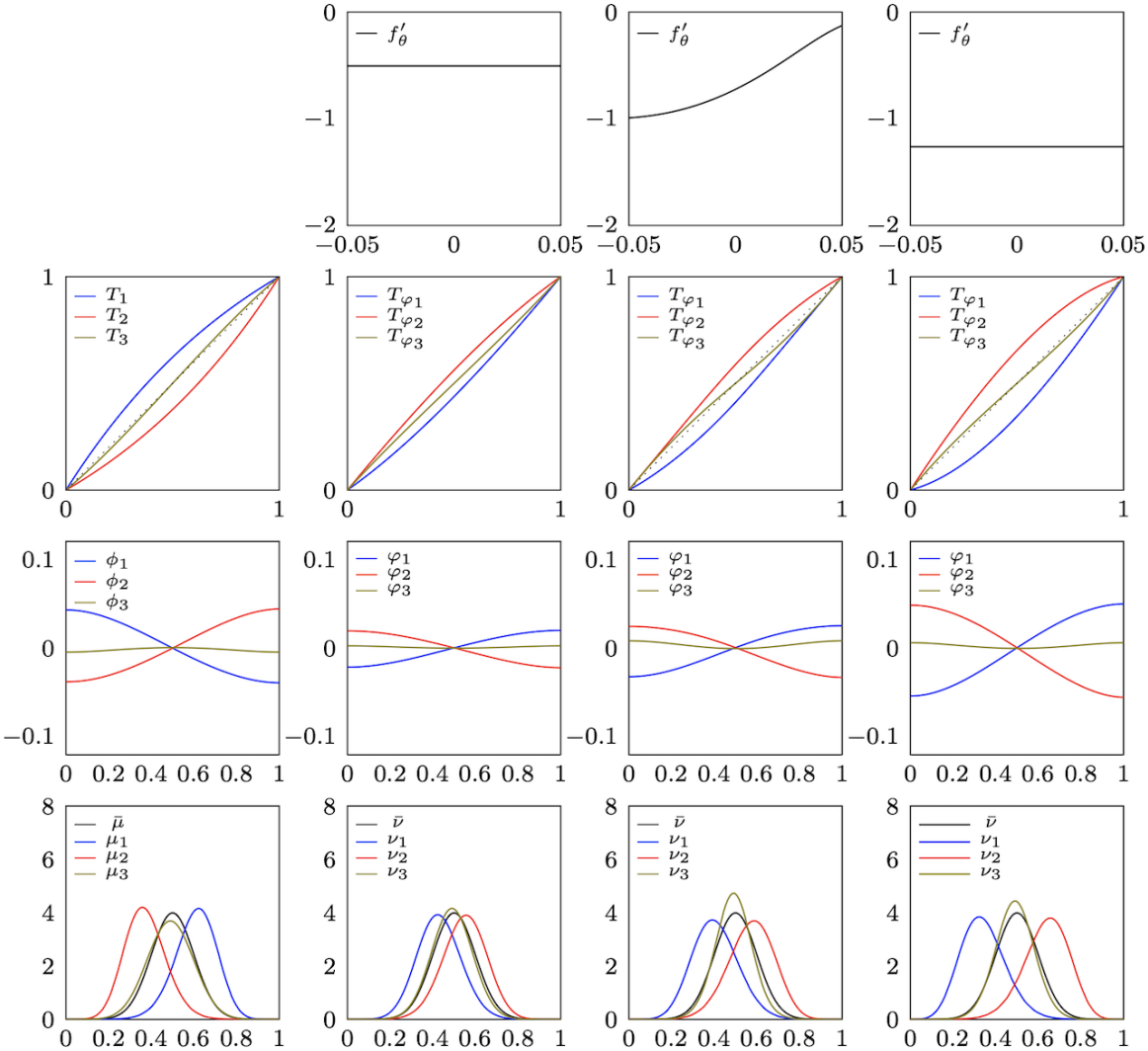


Figure 3: 1D illustration of KR with non-increasing convex functional parameter.

a discrepancy caused by the local deformation induced by the nonlinear $f_\theta$, which cannot occur when the functional parameter $f$ is linear.

Finally, we repeat the experiment but with the functional parameter set as $-f_\theta$. The results are plotted in Figure 3, where we observe that the relative locations of $\mu_1, \mu_2, \mu_3$ with respect to $\bar{\mu}$ are reversed relative to $\nu_1, \nu_2, \nu_3$: $\mu_1$ is on the right while $\nu_1$ is on the left, $\mu_2$ is on the left while $\nu_2$ is on the right, and $\mu_3$ is below $\bar{\mu}$ while $\nu_3$ is above $\bar{\nu}$. In the second column, where $f_\theta(t) = -0.505t$, the $\nu_i$ move closer to $\bar{\nu}$ than the $\mu_i$ are to $\bar{\mu}$. On the other hand, in the fourth column with $f_\theta(t) = -1.2625t$, the $\nu_i$ are farther from $\bar{\nu}$ than the $\mu_i$ are from $\bar{\mu}$. In the third column when $f_\theta$ is nonlinear, we observe a larger effect on $\nu_3$ than

on $\nu_1$ and $\nu_2$ compared to second and fourth column, which can also be seen in the optimal transport map and the Kantorovich potential.

For a 2D example, we let $\mu_1, \mu_2$ be uniform distributions supported on round disks of diameter 0.1 centered at $(0.2, 0.2)$ and $(0.8, 0.8)$ respectively. The Wasserstein barycenter $\bar{\mu}$ of $\mu_1, \mu_2$ is uniform on disk centered at $(0.05, 0, 5)$, and we set $\bar{\nu} = \bar{\mu}$. To illustrate the Kantorovich regression model, we use the same set of functions $f_\theta$ and compute $\varphi_i = f_\theta \circledcirc \phi_{\bar{\mu}\to\mu_i} - \frac{1}{2}\sum_{j=1}^{2} f_\theta \circledcirc \phi_{\bar{\mu}\to\mu_j}$ and $\nu_i = (T_{\varphi_i})_{\#}\bar{\nu}$. In Figure 4, where $f'$ is non-increasing and concave, the relative positions of $\mu_1, \mu_2$ with respect to $\bar{\mu}$ are preserved by $\nu_1, \nu_2$ with respect to $\bar{\nu}$: $\mu_1$ and $\nu_1$ lie in the lower left, and $\mu_2$ and $\nu_2$ lie in the upper right. In the second column, with $f_\theta(t) = 0.505t$, $\nu_1$ and $\nu_2$ are closer to $\bar{\nu}$ than $\mu_1$ and $\mu_2$ are to $\bar{\mu}$. In the fourth column, with $f_\theta(t) = 1.2625t$ , $\nu_1$ and $\nu_2$ are farther from $\bar{\nu}$ than $\mu_1$ and $\mu_2$ are from $\bar{\mu}$. In these cases, the function $f$ scales the length of the displacement vector $T_i(x) - x$ uniformly, yielding uniform distributions. By contrast, in third column, scale $f'_\theta(\phi_i(x))$ varies across $x \in \mathrm{sp}(\bar{\nu})$, so the resulting distributions are not uniform. In Figure 5, where $f'_\theta$ is non-decreasing and convex, the relative positions are reversed: $\mu_1$ (lower left) switches to $\nu_1$ (upper right), while $\mu_2$ (upper right) switches to $\nu_2$ (lower left). Overall, we observe the same effect as in Figure 4, but in the opposite direction.

**Remark 3.4.** *We now discuss the case when* $\mathrm{sp}(\bar{\nu}) \neq \mathrm{sp}(\bar{\mu})$*. By choosing a fixed translation* $\tau : \mathrm{sp}(\bar{\nu}) \to \mathrm{sp}(\bar{\mu})$ *and defining* $\phi_i = \phi_{\bar{\mu}\to\mu_i} \circ \tau$*, model 4 and Theorem 3.2 can be applied in the same way. The only difference is that the constants appearing in Theorem 3.2 must now account for the effect of* $\tau$*. For one-dimensional distributions, if all distributions are supported on connected intervals, then the barycenter is also supported on an interval. Let* $\mathrm{sp}(\bar{\nu}) = [a, b]$ *and* $\mathrm{sp}(\bar{\mu}) = [c, d]$*. We may choose* $\tau$ *to be the affine transformation mapping* $[a, b]$ *to* $[c, d]$*. In this case, composing with* $\tau$ *does not change the shape of* $\phi_{\bar{\mu}\to\mu_i}$*, so the Kantorovich model continues to deform* $\phi_{\bar{\mu}\to\mu_i}$ *only through the model parameters.*

**Remark 3.5.** *In model 4, we impose structural constraints on* $f$*, requiring it to be either non-decreasing and concave or non-increasing and convex. These constraints are motivated by the conditions in Theorem 3.2. In principle, one could allow any* $f \in \mathcal{C}^2(\Omega)$ *as the*

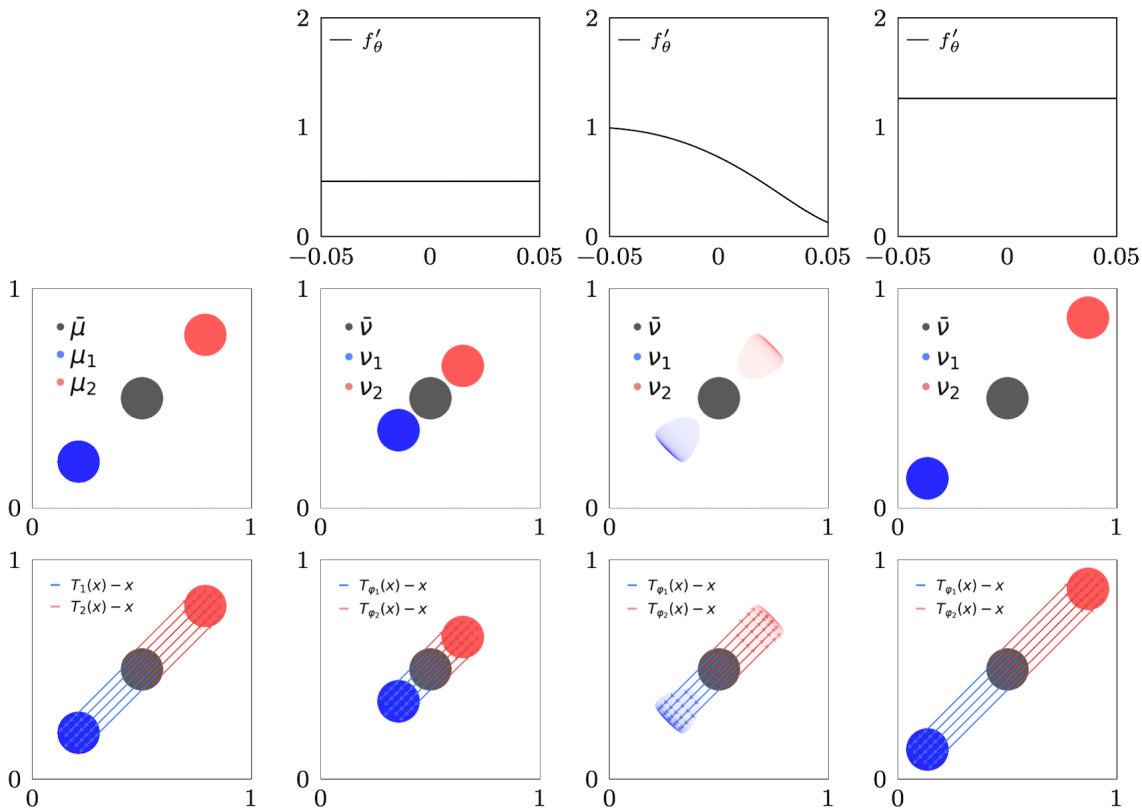


Figure 4: 2D illustration of KR with non-decreasing concave functional parameter.

*functional model parameter and consider the model*

$$\nu_i = (T_{\varepsilon_i})_{\#}\big(T_{f\circ\phi_i - \mathrm{E}[f\circ\phi_i]}\big)_{\#}\bar{\nu}.$$

*The trade-off is that ensuring* $T_{f\circ\phi_i-\mathrm{E}[f\circ\phi_i]}$ *remains c-concave would require stronger bounds on both* $f'$ *and* $f''$*, together with uniform bounds on* $\|\nabla\phi_i(x)\|$ *and* $\|\nabla^2\phi_i(x)\|_{\mathrm{op}}$ *over all* $i$ *and* $x$*, compared to those used in Theorem 3.2.*

### 3.2. Multiple distributional predictors

We now extend the Kantorovich regression (KR) model to incorporate multiple distributional predictors. Let $(\nu, \boldsymbol{\mu}) \sim P_{\nu,\boldsymbol{\mu}}$, where $\boldsymbol{\mu} = (\mu^1, \ldots, \mu^p) \in (\mathcal{P}_{\mathrm{ac}}(\Omega))^p$, and $P_{\nu,\boldsymbol{\mu}}$ is a probability measure on $(\mathcal{P}_{\mathrm{ac}}(\Omega))^{p+1}$. Given an i.i.d. sample $\{(\nu_i, \boldsymbol{\mu}_i)\}_{i=1}^n$ drawn from $P_{\nu,\boldsymbol{\mu}}$, we write $\boldsymbol{\mu}_i = (\mu_i^1, \ldots, \mu_i^p)$. Let $P_\nu$ and $P_{\mu^j}$ denote the marginal distributions of $\nu$ and $\mu^j$, respectively, and let $\bar{\nu}$ and $\bar{\mu}^j$ denote their corresponding population Wasserstein barycenters. Similar

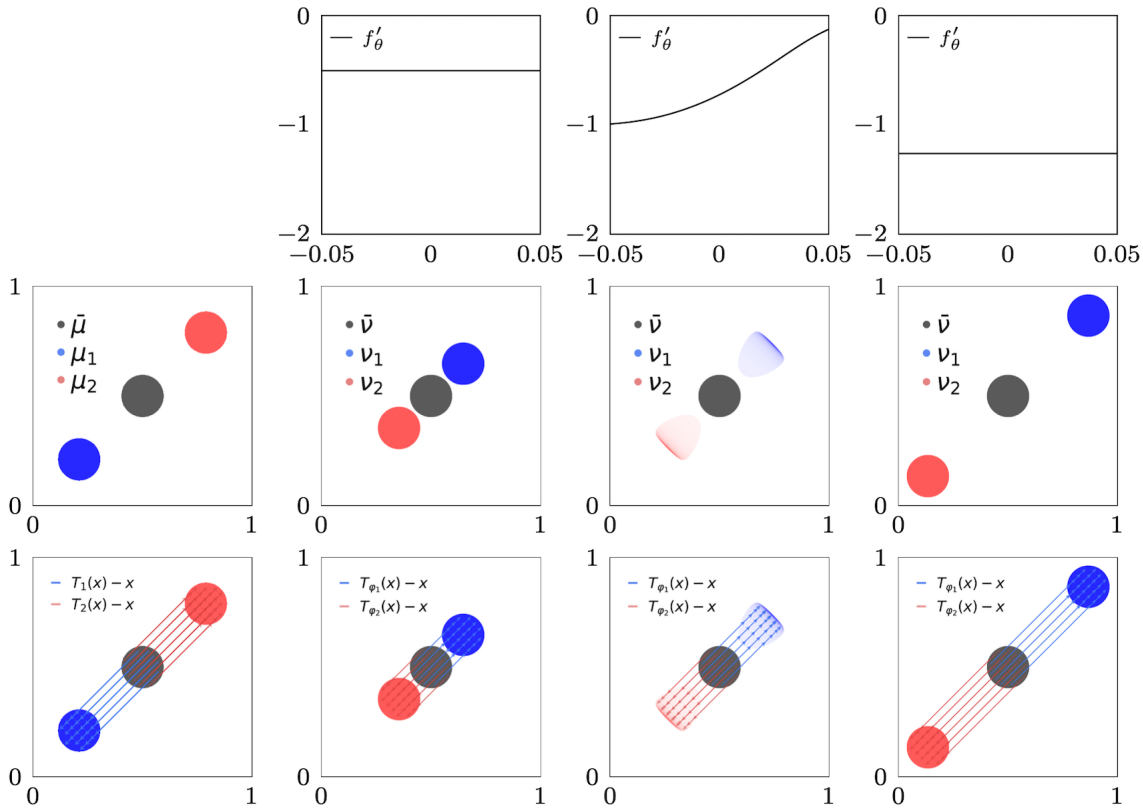


Figure 5: 2D illustration of KR with non-increasing convex functional parameter.

to the one predictor case, we consider $\mathrm{sp}(\bar{\nu}) = \mathrm{sp}(\bar{\mu}^j)$ for all $j$, and define the Kantorovich regression (KR) model with multiple distributional predictors as follows:

$$\nu_i = (T_{\varepsilon_i})_\#(T_{\sum_{j=1}^p \varphi_i^j})_\#\bar{\nu}, \tag{8}$$

where $f_j$ is the functional parameter, $\phi_i^j = \phi_{\bar{\mu}^j \to \mu_i^j}$, $\varphi_i^j = f_j \circledcirc \phi_i^j - \mathrm{E}_{\mu_i^j}[f_j \circledcirc \phi_i^j]$, and $T_{\varepsilon_i}$ is a random transport map with $\mathrm{E}[T_{\varepsilon_i}(x)] = x$. There are $p$ functional parameters, each of which is either non-decreasing and concave or non-increasing and convex. We encode this structure by $\boldsymbol{\delta} = (\delta_1, \ldots, \delta_p)^\top \in \{+, -\}^p$, where $\delta_j = +$ indicates that the $j$th parameter is non-decreasing and concave, and $\delta_j = -$ indicates that it is non-increasing and convex. Let

$$\eta^j := \sup_{x \in \mathrm{sp}(\bar{\nu})} \mathrm{E}_{\mu_i^j}[\|\nabla \phi_i^j(x)\|_2^2], \quad \lambda^j := \sup_{x \in \mathrm{sp}(\bar{\nu})} (\mathrm{E}_{\mu_i^j}[\|\nabla^2 \phi_i^j(x)\|_{\mathrm{op}}^2])^{1/2}$$

and for simplicity of notations, we set $\boldsymbol{\lambda} = (\lambda^1, \ldots, \lambda^p)^\top$, $\boldsymbol{\eta} = (\eta^1, \ldots, \eta^p)^\top$, $\boldsymbol{\kappa}_{1,\boldsymbol{\delta}} = (\kappa^1_{1,\boldsymbol{\delta}}, \ldots, \kappa^p_{1,\boldsymbol{\delta}})^\top$, $\boldsymbol{\kappa}_{2,\boldsymbol{\delta}} = (\kappa^1_{2,\boldsymbol{\delta}}, \ldots, \kappa^p_{2,\boldsymbol{\delta}})^\top$, $\boldsymbol{\gamma}_{\boldsymbol{\delta}} = (\gamma^1_{\delta_1}, \ldots, \gamma^p_{\delta_p})^\top \in \mathbb{R}^p$ and

$$\mathbb{F}_{\boldsymbol{\delta}}(\boldsymbol{\kappa}_{1,\boldsymbol{\delta}}, \boldsymbol{\kappa}_{2,\boldsymbol{\delta}}) = \mathbb{F}_{\delta_1}(\kappa^1_{1,\boldsymbol{\delta}}, \kappa^1_{2,\boldsymbol{\delta}}) \times \cdots \times \mathbb{F}_{\delta_p}(\kappa^p_{1,\boldsymbol{\delta}}, \kappa^p_{2,\boldsymbol{\delta}}).$$

**Corollary 3.6.** *Assuming $\phi^j_i \in \mathbb{K}(\gamma^j_-, \gamma^j_+)$ almost surely, then for each $\boldsymbol{\delta} \in \{+,-\}^p$, by choosing $\boldsymbol{\kappa}_{1,\boldsymbol{\delta}}, \boldsymbol{\kappa}_{2,\boldsymbol{\delta}}$ to satisfy*

$$(\boldsymbol{\gamma}_{\boldsymbol{\delta}}^\top + \boldsymbol{\lambda}^\top)\boldsymbol{\kappa}_{1,\boldsymbol{\delta}} + \boldsymbol{\eta}^\top \boldsymbol{\kappa}_{2,\boldsymbol{\delta}} \leq 1,$$

*the function $\sum_{j=1}^p \varphi^j_i$ is c-concave for any $(f_1, \ldots, f_p) \in \bigcup_{\boldsymbol{\delta} \in \{+,-\}^p} \mathbb{F}_{\boldsymbol{\delta}}(\boldsymbol{\kappa}_{1,\boldsymbol{\delta}}, \boldsymbol{\kappa}_{2,\boldsymbol{\delta}})$.*

For one-dimensional distributions, letting $f_j(t) = \alpha_j t$ and $p = 2$, the KR model (8) simplifies to

$$T_{\bar{\nu} \to \nu_i} = T_{\varepsilon_i} \circ \Big( \mathrm{id} + \alpha_1 \big( T_{\bar{\mu}^1 \to \mu^1_i} - \mathrm{id} \big) + \alpha_2 \big( T_{\bar{\mu}^2 \to \mu^2_i} - \mathrm{id} \big) \Big),$$

where $\alpha_1, \alpha_2 \in \mathbb{R}$. The autoregressive optimal transport model (ATM) proposed in Zhu and Müller, 2023 was developed for distributional time series, but it can also be applied in regression settings. The KR model is structurally different from the ATM model. In particular, the ATM model is defined as

$$T_{\bar{\nu} \to \nu_i} = T_{\varepsilon_i} \circ (\alpha_1 \odot T_{\bar{\mu}^1 \to \mu^1_i}) \circ (\alpha_2 \odot T_{\bar{\mu}^2 \to \mu^2_i}),$$

where $\alpha \odot T = \mathrm{id} + \alpha(T - \mathrm{id})$, if $0 < \alpha < 1$, and $\alpha \odot T = \mathrm{id} + \alpha(\mathrm{id} - T^{-1})$, if $-1 < \alpha < 0$. For $|\alpha| > 1$, let $b = \lfloor |\alpha| \rfloor$ denote the integer part of $|\alpha|$, and set $a = |\alpha| - b$. The operator $\alpha \odot T$ is then defined by

$$\alpha \odot T(x) := \begin{cases} (a \odot T) \circ \underbrace{T \circ T \circ \cdots \circ T}_{b \text{ compositions of } T}(x), & \alpha > 1, \\ (a \odot T^{-1}) \circ \underbrace{T^{-1} \circ T^{-1} \circ \cdots \circ T^{-1}}_{b \text{ compositions of } T^{-1}}(x), & \alpha < -1. \end{cases}$$

Intuitively, the ATM model aggregates multiple predictors through compositions of transport maps, which are noncommutative, whereas KR adopts an additive structure. When the coefficient is negative, the ATM model uses the inverse transport map, while KR instead uses the opposite displacement direction.

### 3.3. Mixed predictor

The problem of predicting a distributional response $\nu_i$ with $q$ Euclidean predictors $\boldsymbol{X}_i = (X_i^1, \ldots, X_i^q)^\top \in \mathbb{R}^q$ is of independent interest. To handle the Euclidean predictor $X_i^k$, the idea is to fit a $c$-concave function $\psi_k$ scaled uniformly by the centered covariate $Z_i^k = X_i^k - \mathrm{E}[X_i^k]$. We define the Kantorovich regression model with Euclidean predictors as

$$\nu_i = (T_{\varepsilon_i})_\# \left( T_{\sum_{k=1}^q Z_i^k \psi_k} \right)_\# \bar{\nu}, \tag{9}$$

where $\{\psi_1, \ldots, \psi_q\}$ are $c$-concave functional parameters.

Consider the case of a single Euclidean predictor $X_i$ ($q = 1$). The model reduces to

$$\nu_i = (T_{\varepsilon_i})_\# \left(T_{Z_i \psi}\right)_\# \bar{\nu} = (T_{\varepsilon_i})_\# \left(\mathrm{id} - Z_i \nabla \psi\right)_\# \bar{\nu},$$

where $Z_i := X_i - \mathrm{E}[X]$. The effect of the Euclidean predictor on the distributional response is governed by the displacement field $-Z_i \nabla \psi(x)$, so that mass is transported locally along the direction $\nabla \psi(x)$ or its opposite depending on the sign of $Z_i$. Specifically, when $Z_i > 0$, mass is displaced in the direction $-\nabla \psi(x)$, whereas when $Z_i < 0$, mass is displaced in the direction $\nabla \psi(x)$. Thus, the Euclidean predictor modulates the response distribution by scaling and reversing the intrinsic transport direction encoded by the potential $\psi$.

For notational convenience, we let $\boldsymbol{l} = (l^1, \ldots, l^q)^\top \in \mathbb{R}^q$, $\boldsymbol{\rho} = (\rho^1, \ldots, \rho^q)^T \in \mathbb{R}^q$ and $\mathbb{K}(\boldsymbol{\rho}, \boldsymbol{\rho}) := \mathbb{K}(\rho^1, \rho^1) \times \cdots \times \mathbb{K}(\rho^q, \rho^q)$. The following theorem characterizes a class of functions $(\psi_1, \ldots, \psi_q)$, determined by the data-generating distribution of $\boldsymbol{X}_i$, that ensures the function $\sum_{k=1}^q Z_i^k \psi_k$ is $c$-concave.

**Theorem 3.7.** *Assuming that $|Z_i^k| \leq l^k$ holds almost surely for all $k$, then by choosing $\boldsymbol{\rho}$ to satisfy*

$$\boldsymbol{l}^\top \boldsymbol{\rho} \leq 1, \tag{10}$$

*we have that the function $\sum_{k=1}^q Z_i^k \psi_k$ is $c$-concave for any $(\psi_1, \ldots, \psi_q) \in \mathbb{K}(\boldsymbol{\rho}, \boldsymbol{\rho})$.*

Let $(\nu, \boldsymbol{\mu}, \boldsymbol{X}) \sim P_{\nu, \boldsymbol{\mu}, \boldsymbol{X}}$, where $P_{\nu, \boldsymbol{\mu}, \boldsymbol{X}}$ is the joint distribution of the random triplet $(\nu, \boldsymbol{\mu}, \boldsymbol{X})$ taking values in the product space $\mathcal{P}_{\mathrm{ac}}(\Omega) \times (\mathcal{P}_{\mathrm{ac}}(\Omega))^p \times \mathbb{R}^q$. The marginal distributions of $\nu, \boldsymbol{\mu}$ and $\boldsymbol{X}$ are denoted as $P_\nu$, $P_{\boldsymbol{\mu}}$ and $P_{\boldsymbol{X}}$ respectively. Given a sample $\{\nu_i, \boldsymbol{\mu}_i, \boldsymbol{X}_i\}_{i=1}^n$ that are i.i.d copies of $(\nu, \boldsymbol{\mu}, \boldsymbol{X})$, we now extend the regression framework

to accommodate $p$ distributional predictors $\boldsymbol{\mu}_i = (\mu_i^1, \ldots, \mu_i^p) \in (\mathcal{P}_{\mathrm{ac}}(\Omega))^p$ and $q$ Euclidean predictors $\boldsymbol{X}_i = (X_i^1, \ldots, X_i^q)^\top \in \mathbb{R}^q$ in predicting a distributional response $\nu_i \in \mathcal{P}_{\mathrm{ac}}(\Omega)$, and define the Kantorovich regression (KR) model with mixed predictors as

$$\nu_i = (T_{\varepsilon_i})_\# \left( T_{\sum_{j=1}^p \varphi_i^j + \sum_{k=1}^q Z_i^k \psi_k} \right)_\# \bar{\nu}, \tag{11}$$

where $\phi_i^j = \phi_{\bar{\mu}^j \to \mu_i^j}$, $\varphi_i^j = f_j \circledcirc \phi_i^j - \mathrm{E}[f_j \circledcirc \phi_i^j]$, and $\boldsymbol{f} = (f_1, \ldots, f_p)^\top, \boldsymbol{\psi} = (\psi_1, \ldots, \psi_q)^\top$ are functional parameters.

By setting $\boldsymbol{\rho}_{\boldsymbol{\delta}} = (\rho_{\boldsymbol{\delta}}^1, \ldots, \rho_{\boldsymbol{\delta}}^q)$, we mean that each component $\rho_{\boldsymbol{\delta}}^k$ depends on the whole $\boldsymbol{\delta}$. Similarly, the corollary below characterizes parameter spaces to ensure $c$-concavity of the predicted potential function.

**Corollary 3.8.** *Assuming that $\phi_i^j \in \mathbb{K}(\gamma_-^j, \gamma_+^j)$ and $|Z_i^k| \leq l^k$ hold almost surely for all $j$ and $k$, then for each $\boldsymbol{\delta} \in \{+, -\}^p$, by choosing $\boldsymbol{\kappa}_{1,\boldsymbol{\delta}}, \boldsymbol{\kappa}_{2,\boldsymbol{\delta}}, \boldsymbol{\rho}_{\boldsymbol{\delta}}$ to satisfy*

$$(\boldsymbol{\gamma}_{\boldsymbol{\delta}}^\top + \boldsymbol{\lambda}^\top)\boldsymbol{\kappa}_{1,\boldsymbol{\delta}} + \boldsymbol{\eta}^\top \boldsymbol{\kappa}_{2,\boldsymbol{\delta}} + \boldsymbol{l}^\top \boldsymbol{\rho}_{\boldsymbol{\delta}} \leq 1, \tag{12}$$

*the function $\sum_{j=1}^p \varphi_i^j + \sum_{k=1}^q Z_i^k \psi_k$ is $c$-concave for any $(\boldsymbol{f}, \boldsymbol{\psi}) \in \cup_{\boldsymbol{\delta} \in \{+,-\}^p} \Theta_{\boldsymbol{\delta}}$, where $\Theta_{\boldsymbol{\delta}} = \mathbb{F}_{\boldsymbol{\delta}}(\boldsymbol{\kappa}_{1,\boldsymbol{\delta}}, \boldsymbol{\kappa}_{1,\boldsymbol{\delta}}) \times \mathbb{K}(\boldsymbol{\rho}_{\boldsymbol{\delta}}, \boldsymbol{\rho}_{\boldsymbol{\delta}})$.*

## 4. Asymptotic Theory

Asymptotic properties of the KR model as the sample size $n \to \infty$ are developed in this section. To apply the model in practice, the population barycenters $\bar{\nu}$ and $\bar{\mu}^j$ are replaced by their empirical counterparts

$$\bar{\nu}_n = \arg \min_{\nu \in \mathcal{P}_{\mathrm{ac}}(\Omega)} \frac{1}{n} \sum_{i=1}^n W_2^2(\nu, \nu_i), \quad \bar{\mu}_n^j = \arg \min_{\mu \in \mathcal{P}_{\mathrm{ac}}(\Omega)} \frac{1}{n} \sum_{i=1}^n W_2^2(\mu, \mu_i^j).$$

Under suitable regularity conditions, the consistency and stability of optimal transport and Wasserstein barycenters have been studied in the literature. For clarity of presentation, we state these properties as assumptions and subsequently discuss relevant references.

**Assumption 4.1.** $W_2(\bar{\nu}_n, \bar{\nu}) = o_p(1)$.

If $d = 1$, this assumption holds straightforwardly. For $d > 1$, under mild regularity conditions on the underlying distributions $P_\nu$, the above assumption holds with convergence

rate $o_p(n^{-1/30})$; see Assumption 1.3 and Theorem 1.7 in Carlier et al., 2024 for details. Faster rates can be obtained under additional structural assumptions. In particular, if the associated Kantorovich potentials are $\alpha$-strongly convex and $\beta$-smooth with $\beta - \alpha < 1$, parametric convergence rates are attainable [Le Gouic et al., 2022].

Given functions $\phi : \Omega \to \mathbb{R}$ and $T : \Omega \to \Omega$, we denote their $L^2(\bar{\nu})$-norm respectively as $\|\phi\|_{L^2(\bar{\nu})} := (\int (\phi(x))^2 \, \mathrm{d}\bar{\nu}(x))^{1/2}$ and $\|T\|_{L^2(\bar{\nu})} := (\int \|T(x)\|^2 \, \mathrm{d}\bar{\nu}(x))^{1/2}$. With a slight abuse of notation, we use the same symbol $\nu$ to denote both a measure and its density when it exists. The sup-norm of a density $\nu$ is defined by $\|\nu\|_\infty := \sup_{x \in \mathrm{sp}(\nu)} \nu(x)$.

The following assumption is related to the consistency of $\bar{\mu}_n^j$ and the quantitative stability properties of the associated optimal transport maps.

**Assumption 4.2.** *For all $i, j$, the potentials $\phi_{\bar{\mu}_n^j \to \mu_i^j}$ are continuously differentiable, and*

$$\frac{1}{n} \sum_{i=1}^{n} \|\phi_{\bar{\mu}_n^j \to \mu_i^j} - \phi_{\bar{\mu}^j \to \mu_i^j}\|_{L^2(\bar{\nu}_n)} = o_p(1), \tag{13}$$

$$\frac{1}{n} \sum_{i=1}^{n} \|\nabla\phi_{\bar{\mu}_n^j \to \mu_i^j} - \nabla\phi_{\bar{\mu}^j \to \mu_i^j}\|_{L^2(\bar{\nu}_n)} = o_p(1). \tag{14}$$

The assumption is readily satisfied for one-dimensional distributions. In higher dimensions, assume that the densities of $\bar{\nu}_n$ are uniformly bounded, i.e., $\sup_n \|\bar{\nu}_n\|_\infty \leq c_1 < \infty$. Then, the $L^2(\bar{\nu}_n)$-norm is controlled by the $L^2(\Omega)$-norm, and thus the quantities in (13)–(14) can be upper bounded by their corresponding $L^2(\Omega)$-norms. Recall that $\phi_{\bar{\mu}_n^j \to \mu_i^j}, \phi_{\bar{\mu}^j \to \mu_i^j}$ are centered so that $\int \phi_{\bar{\mu}_n^j \to \mu_i^j} \, \mathrm{d}\bar{\nu}_n = 0$, $\int \phi_{\bar{\mu}^j \to \mu_i^j} \, \mathrm{d}d\bar{\nu} = 0$ respectively. Under suitable regularity conditions (e.g., uniform lipschitzness) on $\phi_{\bar{\mu}_n^j \to \mu_i^j}$, a Poincaré-type inequality on $\Omega$ implies for some constant $c_2$,

$$\left\|\phi_{\bar{\mu}_n^j \to \mu_i^j} - \phi_{\bar{\mu}^j \to \mu_i^j}\right\|_{L^2(\Omega)} \leq c_2 \left\{ \left\|\nabla\phi_{\bar{\mu}_n^j \to \mu_i^j} - \nabla\phi_{\bar{\mu}^j \to \mu_i^j}\right\|_{L^2(\Omega)} + W_2(\bar{\nu}_n, \bar{\nu}) \right\},$$

where the $W_2(\bar{\nu}_n, \bar{\nu})$ term accounts for possible differences in centering with respect to $\bar{\nu}_n$ and $\bar{\nu}$. Furthermore, Theorem 1.4 of Berman, 2021 yields

$$\|\nabla\phi_{\bar{\mu}_n^j \to \mu_i^j} - \nabla\phi_{\bar{\mu}^j \to \mu_i^j}\|_{L^2(\Omega)} \leq c_3 \, W_1(\bar{\mu}_n^j, \bar{\mu}^j)^{1/2^d},$$

for some constant $c_3$ independent of $i$. As a consequence, Assumption 4.2 holds whenever $W_2(\bar{\nu}_n, \bar{\nu}) = o_p(1)$ and $W_1(\bar{\mu}_n^j, \bar{\mu}^j) = o_p(1)$ for all $j$.

Given a sample $\{\nu_i, \boldsymbol{\mu}_i, \boldsymbol{X}_i\}_{i=1}^n$, the intercept term $\mathrm{E}[f_j \circledcirc \phi_i^j]$ and $\mathrm{E}[X_i^k]$ are estimated by their sample averages $\frac{1}{n}\sum_{i=1}^n f_j \circledcirc \widehat{\phi}_i^j$ and $\frac{1}{n}\sum_{i=1}^n X_i^k$, respectively, where $\widehat{\phi}_i^j = \phi_{\bar{\mu}_n^j \to \mu_i^j}$. The functional parameters are estimated by minimizing the empirical Wasserstein loss

$$\widehat{L}(\boldsymbol{f}, \boldsymbol{\psi}) := \frac{1}{n}\sum_{i=1}^n W_2^2\big(\nu_i, (T_{\sum_{j=1}^p \widehat{\varphi}_i^j + \sum_{k=1}^q \widehat{Z}_i^k \psi_k})_{\#}\bar{\nu}_n\big),$$

where $\widehat{\varphi}_i^j = f_j \circledcirc \widehat{\phi}_i^j - \frac{1}{n}\sum_{k=1}^n f_j \circledcirc \widehat{\phi}_k^j$ and $\widehat{Z}_i^k = X_i^k - \frac{1}{n}\sum_{j=1}^n X_j^k$. Its population counterpart is defined by

$$L(\boldsymbol{f}, \boldsymbol{\psi}) := \mathrm{E}\left[W_2^2\Big(\nu_1,\ \big(T_{\sum_{j=1}^p \varphi_1^j + \sum_{k=1}^q Z_1^k \psi_k}\big)_{\#}\bar{\nu}\Big)\right].$$

If $\nu_1$ is generated from model 11 with true parameter $(\check{\boldsymbol{f}}, \check{\boldsymbol{\psi}})$, and the random map $T_{\varepsilon_1}$ is cyclically monotone and satisfies that $\mathrm{E}[T_{\varepsilon_1}(x)] = x$, then $(\check{\boldsymbol{f}}, \check{\boldsymbol{\psi}})$ is a minimizing pair of $L(\boldsymbol{f}, \boldsymbol{\psi})$. The following theorem establishes the uniform convergence of $\widehat{L}$ to $L$ over $\cup_{\boldsymbol{\delta}\in\{+,-\}^p}\Theta_{\boldsymbol{\delta}}$. We note that the inequality 12 is used to enforce intrinsic structure of the model, and is not needed here.

**Theorem 4.3.** *Under Assumptions 4.1, 4.2. Assuming that $\phi_i^j \in \mathbb{K}(\gamma_-^j, \gamma_+^j)$, $|Z_i^k| \le l^k$ hold almost surely for all $j$ and $k$, and for each $\boldsymbol{\delta} \in \{+,-\}^p$, the vectors $\boldsymbol{\kappa}_{1,\boldsymbol{\delta}}, \boldsymbol{\kappa}_{2,\boldsymbol{\delta}}, \boldsymbol{\rho}_{\boldsymbol{\delta}}$ are bounded. Then, we have*

$$\sup_{(\boldsymbol{f},\boldsymbol{\psi})\in\cup_{\boldsymbol{\delta}\in\{+,-\}^p}\Theta_{\boldsymbol{\delta}}} \left|\widehat{L}(\boldsymbol{f}, \boldsymbol{\psi}) - L(\boldsymbol{f}, \boldsymbol{\psi})\right| = o_p(1).$$

The above uniform convergence result, together with the separation condition for the minimizer of $L$ as in Corollary 3.2.3 of Van der Vaart and Wellner, 2023, implies the consistency of the empirical estimator

$$(\widehat{\boldsymbol{f}}, \widehat{\boldsymbol{\psi}}) \in \arg\min_{\cup_{\boldsymbol{\delta}}\Theta_{\boldsymbol{\delta}}} \widehat{L}(\boldsymbol{f}, \boldsymbol{\psi}).$$

In the one-dimensional setting, the population loss admits the quadratic form

$$L(\boldsymbol{f}, \boldsymbol{\psi}) := \mathrm{E}\Big[\int_\Omega \Big(T_{\bar{\nu}\to\nu}(x) - x + \sum_{j=1}^p (\varphi^j)'(x) + \sum_{k=1}^q Z^k \psi_k'(x)\Big)^2 \mathrm{d}\bar{\nu}(x)\Big],$$

where $\bar{\nu}$ is the population barycenter, $Z^k := X^k - \mathrm{E}[X^k]$, and $\phi^j = \phi_{\bar{\mu}^j \to \mu^j}, \varphi^j = f_j \circledcirc \phi^j - \mathrm{E}\left[f_j \circledcirc \phi^j\right]$. The objective is convex in $(\boldsymbol{f}, \boldsymbol{\psi})$. Moreover, uniqueness of the minimizer over

$\Theta_{\boldsymbol{\delta}}$ for each fixed $\boldsymbol{\delta}$ follows from the following non-degeneracy condition: for any $(\boldsymbol{g}, \boldsymbol{h}) \in \Theta_{\boldsymbol{\delta}}$,

$$\mathrm{E}\Big[\int_{\Omega}\Big(\sum_{j=1}^{p}\big(g_j \circledcirc \phi^j - \mathrm{E}[g_j \circledcirc \phi^j]\big)'(x) + \sum_{k=1}^{q} Z^k\, h_k'(x)\Big)^2 \mathrm{d}\bar{\nu}(x)\Big] = 0$$

implies $g_j' = 0$ for all $j$ and $h_k' = 0$ for all $k$. Under this condition, the quadratic objective is strictly convex and therefore admits a unique minimizer over $\Theta_{\boldsymbol{\delta}}$ for each fixed $\boldsymbol{\delta}$. Let $\check{\boldsymbol{\delta}}$ be such that $\check{\boldsymbol{f}} \in \Theta_{\check{\boldsymbol{\delta}}}$. Assuming that $\check{\boldsymbol{f}} = (\check{f}_1, \ldots, \check{f}_p)$ is non-degenerate, i.e., $\check{f}_j$ is not a constant for any $j$ and $L(\check{\boldsymbol{f}}, \check{\boldsymbol{\psi}}) < \min_{(\boldsymbol{f},\boldsymbol{\psi})\in\Theta_{\boldsymbol{\delta}}} L(\boldsymbol{f}, \boldsymbol{\psi})$ for any $\boldsymbol{\delta} \neq \check{\boldsymbol{\delta}}$. Then, $L(\boldsymbol{f}, \boldsymbol{\psi})$ satisfies the separation condition in Corollary 3.2.3 [Van der Vaart and Wellner, 2023] and the estimator $(\widehat{\boldsymbol{f}}, \widehat{\boldsymbol{\psi}})$ converges in outer probability to $(\check{\boldsymbol{f}}, \check{\boldsymbol{\psi}})$.

For multivariate distributions, the population objective $L(\boldsymbol{f}, \boldsymbol{\psi})$ is generally non-convex. Consequently, uniqueness of the minimizer cannot be guaranteed via convexity arguments and may not hold in general. Rather than establishing convergence of the estimator $(\widehat{\boldsymbol{f}}, \widehat{\boldsymbol{\psi}})$, we derive consistency in terms of excess risk.

**Corollary 4.4.** *Under the same assumptions of Theorem 4.3, we have*

$$\big|L(\widehat{\boldsymbol{f}}, \widehat{\boldsymbol{\psi}}) - L(\check{\boldsymbol{f}}, \check{\boldsymbol{\psi}})\big| = o_p(1).$$

## 5. Computational Algorithms

In this section, we develop first-order gradient-based algorithms for minimizing the empirical objective $\widehat{L}(\boldsymbol{f}, \boldsymbol{\psi})$. As a preliminary step, we build upon recent gradient-based methods for optimal transport and Wasserstein barycenters [Jacobs et al., 2021; Kim et al., 2025, 2026] to establish the differential structure of the functional $G(\phi) := \frac{1}{2}W_2^2\big(\nu, (T_\phi)_{\#}\bar{\nu}\big)$.

**Lemma 5.1.** *The Gâteaux derivative of $G$ at $\phi$ in the direction $h$, denoted by $\delta G_\phi(h)$, is*

$$\delta G_\phi(h) := \frac{\mathrm{d}}{\mathrm{d}\varepsilon} G(\phi + \varepsilon h)\Big|_{\varepsilon=0} = -\int \big\langle \nabla\phi_{(T_\phi)_{\#}\bar{\nu}\to\nu}\big(T_\phi(x)\big),\, \nabla h(x)\big\rangle\, \mathrm{d}\bar{\nu}(x).$$

*Since $G(\phi)$ depends on $\phi$ though $\nabla\phi$ only, we conclude that the $L^2(\bar{\nu})$-gradient of $G$ at $\nabla\phi$ is $-\nabla\phi_{(T_\phi)_{\#}\bar{\nu}\to\nu_i} \circ T_\phi$.*

Lemma 5.1 provides the fundamental building block for our algorithm. Now consider $R(f) := \frac{1}{2}W_2^2\big(\nu, (T_\Psi)_{\#}\bar{\nu}\big)$, where $\Psi = f \circ \phi$. Observing that $\delta\Psi_f(h) = h \circ \phi$, and $R(f) =$

$G(f \circ \phi)$. Applying the chain rule yields

$$\begin{aligned}\delta R_f(h) &= \delta G_\Psi(\delta \Psi_f(h)) \\ &= -\int \left\langle \nabla \phi_{(T_\Psi)_\# \bar{\nu} \to \nu}\big(T_\Psi(x)\big),\, \nabla (h \circ \phi)(x) \right\rangle \mathrm{d}\bar{\nu}(x) \\ &= -\int h'(\phi(x)) \left\langle \nabla \phi_{(T_\Psi)_\# \bar{\nu} \to \nu}\big(T_\Psi(x)\big),\, \nabla \phi(x) \right\rangle \mathrm{d}\bar{\nu}(x),\end{aligned}$$

where we used $\nabla(h \circ \phi)(x) = h'(\phi(x))\, \nabla \phi(x)$. Furthermore, we let $\{\bar{\nu}_t\}$ be the disintegration of $\bar{\nu}$ with respect to $\phi$, then $\delta R_f(h) = -\int h'(t) \Gamma_{\Psi,\phi}(t)\, \mathrm{d}(\phi_\# \bar{\nu})(t)$, where

$$\Gamma_{\Psi,\phi}(t) = \int \left\langle \nabla \phi_{(T_\Psi)_\# \bar{\nu} \to \nu}\big(T_\Psi(x)\big),\, \nabla \phi(x) \right\rangle \mathrm{d}\bar{\nu}_t(x).$$

Since $R(f)$ depends on $f$ though $f'$ only, we conclude that the gradient of $R$ at $f'$ is $-\Gamma_{\Psi,\phi}$ in $L^2(\phi_\# \bar{\nu})$. Next, we define $\widehat{\Phi}_i(x) := \sum_{j=1}^p \widehat{\varphi}_i^j(x) + \sum_{k=1}^q \widehat{Z}_i^k \psi_k(x)$, $\widehat{\nu}_i = (T_{\widehat{\Phi}_i})_\# \bar{\nu}_n$, and

$$\widehat{\Gamma}_{\widehat{\Phi}_i, \phi_i^j}(t) = \int \left\langle \nabla \phi_{\widehat{\nu}_i \to \nu_i}\big(T_{\widehat{\Phi}_i}(x)\big) - \frac{1}{n} \sum_{r=1}^n \nabla \phi_{\widehat{\nu}_r \to \nu_r}\big(T_{\widehat{\Phi}_r}(x)\big), \nabla \phi_i^j(x) \right\rangle \mathrm{d}\bar{\nu}_{n,t}(x),$$

where $\{\bar{\nu}_{n,t}\}$ denote the family of conditional measures obtained by disintegrating $\bar{\nu}_n$ with respect to $\phi_i^j$ when $f_j$ is non-decreasing and concave, and with respect to $-\phi_i^j$ when $f_j$ is non-increasing and convex. The same approach can be used to compute the gradient of $\widehat{L}(\boldsymbol{f}, \boldsymbol{\psi})$ at each $f_j$ or $\psi_k$ as formalized below.

**Theorem 5.2.** *(i) $\widehat{L}$ depends on $f_j$ only through $f_j'$. The Gâteaux derivative of $\widehat{L}$ at $f_j'$ in the direction $h'$ is*

$$\delta(\widehat{L})_{f_j}(h) = \begin{cases} -\frac{2}{n} \sum_{i=1}^n \int h'(t) \widehat{\Gamma}_{\widehat{\Phi}_i, \phi_i^j}(t)\, \mathrm{d}(\phi_i^j)_\# \bar{\nu}_n(t), & f_j \text{ non-decreasing concave}, \\ \frac{2}{n} \sum_{i=1}^n \int h'(t) \widehat{\Gamma}_{\widehat{\Phi}_i, -\phi_i^j}(t)\, \mathrm{d}(-\phi_i^j)_\# \bar{\nu}_n(t), & f_j \text{ non-increasing convex}. \end{cases}$$

*Thus, the $L^2([a,b])$-gradient of $\widehat{L}$ at $f_j'$ is $-2/n \sum_{i=1}^n ((\phi_i^j)_\# \bar{\nu}_n) \widehat{\Gamma}_{\widehat{\Phi}_i, \phi_i^j}$ when $f_j$ is non-decreasing and convex, and $2/n \sum_{i=1}^n ((-\phi_i^j)_\# \bar{\nu}_n) \widehat{\Gamma}_{\widehat{\Phi}_i, -\phi_i^j}$ when $f_j$ is non-increasing and convex.*

*(ii) $\widehat{L}$ depends on $\psi_k$ only through $\nabla \psi_k$. The Gâteaux derivative of $\widehat{L}$ at $\psi_k$ in the direction $h$ is*

$$\delta(\widehat{L})_{\psi_k}(h) = -\frac{2}{n} \sum_{i=1}^n \int \langle \nabla \phi_{\hat{\nu}_i \to \nu_i}(T_{\Phi_i}(x)), \nabla h(x) \rangle\, \mathrm{d}\bar{\nu}_n.$$

*Thus, the $L^2(\bar{\nu}_n)$-gradient of $\widehat{L}$ at $\nabla \psi_k$ is $-2/n \sum_{i=1}^n \nabla \phi_{\hat{\nu}_i \to \nu_i}(T_{\Phi_i})$.*

To compute the gradient numerically, one natural approach is to discretize the infinite-dimensional objects, including $\bar{\nu}_n$, $f_j$, and $\psi_k$, on a regular grid over $\Omega$, and approximate the gradient operator using finite-difference schemes. The pushforward operation can then be implemented by evaluating the transport map on the discretized grid, followed by an appropriate interpolation or mass-redistribution step to construct the transported measure. We refer to Jacobs et al., 2021; Kim et al., 2025, 2026 for more details on numerical implementations along these lines.

Alternatively, instead of working directly in function space, we may parameterize the derivative $f_j'$ via a finite-dimensional representation. Let $\mathbb{R}_+$ and $\mathbb{R}_-$ denote the sets of nonnegative and nonpositive real numbers, respectively. We consider the following piecewise-constant parameterization.

$$f'_{\boldsymbol{\theta}_j}(t) = \sum_{l=1}^{K} \theta_{j,l} \mathbf{1}_{\{t \le z_l\}}, \tag{15}$$

where $\boldsymbol{\theta}_j = (\theta_{j,1}, \ldots, \theta_{j,K})^T \in (\mathbb{R}_+)^K$ for non-decreasing and concave $f_j$, and $\boldsymbol{\theta}_j \in (\mathbb{R}_-)^K$ for non-increasing and convex $f_j$. For the $c$-concave function $\psi_k$, we note that $\psi_k = \frac{\|x\|_2^2}{2} - h(x)$ for some convex function $h : \Omega \to \mathbb{R}$. Thus, one-dimensional $\psi_k'$ can be parametrized by $\psi'_{\boldsymbol{\vartheta}_k}$,

$$\psi'_{\boldsymbol{\vartheta}_k}(x) = x - \sum_{l=1}^{K} \vartheta_{k,l} \mathbf{1}_{\{x \ge z_l\}}, \tag{16}$$

where $\boldsymbol{\vartheta}_k = (\vartheta_{k,1}, \ldots, \vartheta_{k,K})^T \in (\mathbb{R}_+)^K$. For the multivariate case, $\psi_k$ can be parametrized using convexity-preserving model such as input-convex neural network (ICNN) [Amos et al., 2017]. Define $\widehat{J}(\boldsymbol{\theta}_1, \ldots, \boldsymbol{\theta}_p, \boldsymbol{\vartheta}_1, \ldots, \boldsymbol{\vartheta}_q) := \widehat{L}(f_{\boldsymbol{\theta}_1}, \ldots, f_{\boldsymbol{\theta}_p}, \psi_{\boldsymbol{\vartheta}_1}, \ldots, \psi_{\boldsymbol{\vartheta}_q})$, the following theorem gives formulas for gradient of $\widehat{J}$ with respect to $\boldsymbol{\theta}_j$ and $\boldsymbol{\vartheta}_k$.

**Theorem 5.3.** *Let $\widehat{\Phi}_i$ and $\widehat{\nu}_i$ be defined in the same way as before, except that we now have $f_j = f_{\boldsymbol{\theta}_j}$ and $\psi_k = \psi_{\boldsymbol{\vartheta}_k}$.*

*(i) The partial derivative of $\widehat{J}$ with respect to $\theta_{j,l}$ is*

$$\frac{\partial \widehat{J}}{\partial \theta_{j,l}} = \begin{cases} -\frac{2}{n} \sum_{i=1}^{n} \int \left\langle \Delta_i(x), \nabla \phi_i^j(x) \right\rangle \mathbf{1}_{\left\{\phi_i^j(x) \le z_l\right\}} \mathrm{d}\bar{\nu}_n(x), & \text{if } \boldsymbol{\theta}_j \in (\mathbb{R}_+)^K; \\ -\frac{2}{n} \sum_{i=1}^{n} \int \left\langle \Delta_i(x), \nabla \phi_i^j(x) \right\rangle \mathbf{1}_{\left\{-\phi_i^j(x) \le z_l\right\}} \mathrm{d}\bar{\nu}_n(x), & \text{if } \boldsymbol{\theta}_j \in (\mathbb{R}_-)^K. \end{cases}$$

*where $\Delta_i(x) = \nabla \phi_{\widehat{\nu}_i \to \nu_i}(T_{\widehat{\Phi}_i}(x)) - \frac{1}{n} \sum_{r=1}^{n} \nabla \phi_{\widehat{\nu}_r \to \nu_r}(T_{\widehat{\Phi}_r}(x))$.*

*(ii) For the one-dimensional case, the partial derivative of $\widehat{J}$ with respect to $\vartheta_{k,l}$ is*

$$\frac{\partial \widehat{J}}{\partial \vartheta_{k,l}} = \frac{2}{n}\sum_{i=1}^{n}\int (T_{\widehat{\Phi}_i}(x) - T_{\bar{\nu}_n \to \nu_i}(x))\mathbf{1}_{\{x \geq z_l\}}\mathrm{d}\bar{\nu}_n(x).$$

The parametrization of $\psi_k$ in 16 is used only for the univariate setting, while the parametrization of $f_j$ in 15 applies to both univariate and multivariate case. In one dimension, the partial derivative of $\widehat{J}$ w.r.t $\vartheta_{k,l}$ can be simplified since now $T_{\hat{\nu}_i \to \nu_i}(T_{\hat{\Phi}_i}(x)) = T_{\bar{\nu}_n \to \nu_i}(x)$ and

$$\Delta_i(x) = T_{\hat{\Phi}_i}(x) - T_{\bar{\nu}_n \to \nu_i}(x) - \frac{1}{n}\sum_{i=1}^{n}(T_{\hat{\Phi}_i}(x) - T_{\bar{\nu}_n \to \nu_i}(x)) = T_{\hat{\Phi}_i}(x) - T_{\bar{\nu}_n \to \nu_i}(x).$$

Likewise, in the univariate case we obtain a simpler expression for the partial derivative of $\widehat{J}$ with respect to $\theta_{j,l}$:

$$\frac{\partial \widehat{J}}{\partial \theta_{j,l}} = \begin{cases} -\frac{2}{n}\sum_{i=1}^{n}\int \left\langle T_{\widehat{\Phi}_i}(x) - T_{\bar{\nu}_n \to \nu_i}(x), \nabla\phi_i^j(x)\right\rangle \mathbf{1}_{\left\{\phi_i^j(x) \leq z_l\right\}}\mathrm{d}\bar{\nu}_n(x), & \text{if } \boldsymbol{\theta}_j \in (\mathbb{R}_+)^K; \\ -\frac{2}{n}\sum_{i=1}^{n}\int \left\langle T_{\widehat{\Phi}_i}(x) - T_{\bar{\nu}_n \to \nu_i}(x), \nabla\phi_i^j(x)\right\rangle \mathbf{1}_{\left\{-\phi_i^j(x) \leq z_l\right\}}\mathrm{d}\bar{\nu}_n(x), & \text{if } \boldsymbol{\theta}_j \in (\mathbb{R}_-)^K. \end{cases}$$

Estimation of the model parameters is performed separately for each fixed $\boldsymbol{\delta} \in \{+,-\}^p$, and the configuration that achieves the smallest loss is subsequently selected. Recall that $\delta_j$ specifies whether $f_j$ is non-decreasing and concave or non-increasing and convex, and therefore determines whether whether $\boldsymbol{\theta}_j \in (\mathbb{R}_+)^K$ or $\boldsymbol{\theta}_j \in (\mathbb{R}_-)^K$. For each $\boldsymbol{\delta}$, the objective $\widehat{J}$ reduces to a quadratic function of $\{\boldsymbol{\theta}_j\}$ and $\{\boldsymbol{\vartheta}_k\}$ in the univariate setting. In this case, the minimizer of $\widehat{J}$ over $\Pi_{j=1}^p \mathbb{R}_{\delta_j}^K \times (\mathbb{R}_+)^{qK}$ can be computed using standard projected gradient descent for each $\boldsymbol{\delta} \in \{+,-\}^p$, which attains an algorithmic convergence rate of order $O(1/T)$. For multivariate distributions, $\nabla\psi_k$ can be parameterized as

$$\nabla\psi_{\boldsymbol{\vartheta}_k}(x) = x - \nabla_x \mathrm{ICNN}(x \mid \boldsymbol{\vartheta}_k),$$

where $\mathrm{ICNN}(x \mid \boldsymbol{\vartheta}_k)$ is an input-convex neural network that is convex in $x$ but potentially nonconvex in $\boldsymbol{\vartheta}_k$ [Amos et al., 2017]. In this setting, standard gradient descent algorithms can still be employed to minimize $\widehat{J}$. However, global algorithmic convergence is no longer guaranteed due to the nonconvexity of $\mathrm{ICNN}(x \mid \boldsymbol{\vartheta}_k)$ with respect to $\boldsymbol{\vartheta}_k$.

## 6. Numerical Studies

The proposed KR model is illustrated using one-dimensional distributions with mixed predictors and two-dimensional distributions with a distributional predictor.

### 6.1. 1D synthetic data

We set the distributional predictors $\mu_i^1$ and $\mu_i^2$ as distributions obtained by truncating probability density functions of $\mathcal{N}(m_i^1, (\sigma_i^1)^2)$ and $\mathcal{N}(m_i^2, (\sigma_i^2)^2)$ to $[0,1]$, respectively. Here, $\{m_i^1\} \sim^{i.i.d} \text{Unif}[0.2, 0.5]$, $\{m_i^2\} \sim^{i.i.d} \text{Unif}[0.5, 0.8]$, $\sigma_1^i \sim^{i.i.d} \text{Unif}[0.2, 0.3]$, and $\sigma_2^i \sim^{i.i.d} \text{Unif}[0.3, 0.4]$. The associated true functional parameters $\check{f}_1$ and $\check{f}_2$ are chosen such that $\check{f}_1'(x) = 0.5(1-x)^{1/2}$ and $\check{f}_2'(x) = 0.5\log(1.2-x)$. The random distortion maps are generated by $T_{\varepsilon_i}(x) = x + \sum_{k=1}^{10} \xi_i^k \sin(k\pi x)$ and $\xi_i^k \sim^{i.i.d} \text{Unif}\left[-\frac{1}{55\pi}, \frac{1}{55\pi}\right]$. This construction ensures that $T_{\varepsilon_i}$ are non-decreasing random functions satisfying $\mathrm{E}[T_{\varepsilon_i}] = \mathrm{id}$. As for the Euclidean predictor, we take $X_i \sim \text{Unif}[0,1]$ and use the $c$-concave function $\check{\psi}(x) = 0.3\left(\frac{x}{2\pi} - \frac{\sin(2\pi x)}{4\pi^2}\right)$ as true parameter. The random distributions $\{\nu_i\}$ are generated according to

$$\nu_i = (T_{\varepsilon_i})_{\#}\left(T_{\tilde{\varphi}_i^1 + \tilde{\varphi}_i^2 + Z_i\check{\psi}}\right)_{\#}\bar{\nu}, \tag{17}$$

where, for $j = 1, 2$, each $\phi_i^j$ is chosen so that $(\phi_i^j)'(x) = x - F_{\mu_i^j}^{-1}(F_{\bar{\mu}_n^j}(x))$ and $\int_0^1 \phi_i^j(x)\,\mathrm{d}x = 0$, and $\tilde{\varphi}_i^j = \check{f}_1 \circ \phi_i^j - \frac{1}{n}\sum_{r=1}^n \check{f}_1 \circ \phi_r^j$. Based on the generated sample $\{\nu_i, (\mu_i^1, \mu_i^2), Z_i\}_{i=1}^n$, the true model parameters $(\check{f}_1, \check{f}_2, \check{\psi})$ are estimated by minimizing $\widehat{L}$ using algorithms introduced in Section 5. Figure 6 displays the logarithm of the $L^2$-distance between the true derivatives $(\check{f}_1', \check{f}_2', \check{\psi}')$ and their estimators $(\widehat{f}_1', \widehat{f}_2', \widehat{\psi}')$ as a function of $\log(n)$, demonstrating convergence of the estimators as $n$ grows.

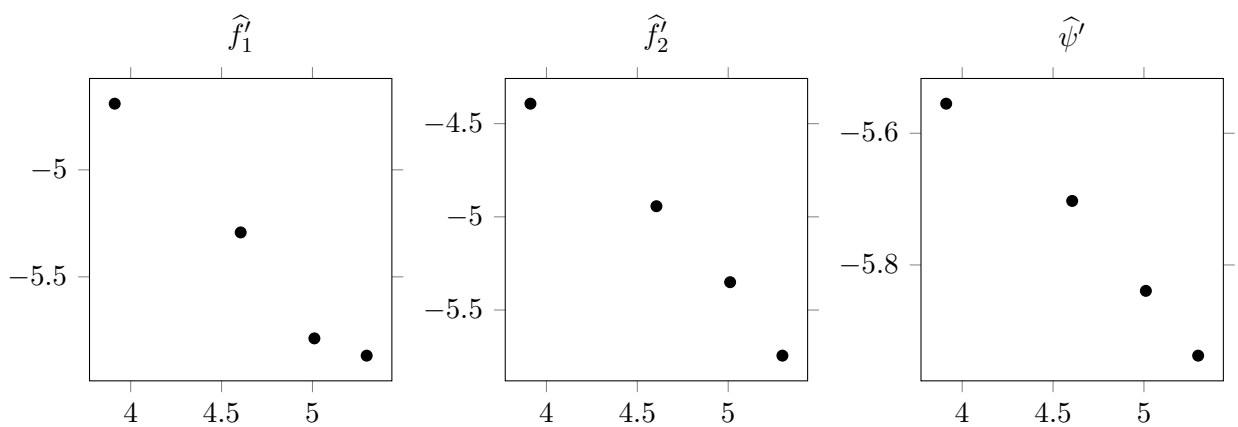


Figure 6: Plot of the logarithm of the $L^2$ estimation error versus $\log(n)$ for the Kantorovich regression model with mixed predictors in (17).

### 6.2. 1D real data

In housing market, sale prices are realized after search, bargaining, and financing, their distribution ($\nu$) should be a deformation of the listing distribution ($\mu$), encoding sellers' initial offers. The mortgage rate ($X$) shapes buyers' purchasing power and bidding intensity: higher rates tighten affordability and shift mass in $\nu$ toward lower prices, whereas lower rates ease constraints and push the distribution rightward. In light of these mechanisms, we predict the monthly density $\nu$ of median sale prices for single-family residences (SFRs) across U.S. metropolitan areas over March 2018-December 2024, using predictors $(\mu_i, X_i)$ available between January 2018 and October 2024. Here, we denote $\mu_i$ and $X_i$ as the listing-price density for SFR and the mortgage rate observed two months prior to $\nu_i$ (with $X_i$ measured in %). We model the relationship between $\nu_i$ and $(\mu_i, X_i)$ by the proposed Kantorovich regression with mixed predictors:

$$\nu_i = (T_{\varepsilon_i})_{\#}\left(T_{\check{f}\circledcirc\phi_{\bar{\mu}\to\mu_i} - \mathrm{E}[\check{f}\circledcirc\phi_{\bar{\mu}\to\mu_i}] + Z_i\check{\psi}}\right)_{\#}\bar{\nu}. \tag{18}$$

Monthly median sale and listing price series for SFR for all metropolitan areas in the US are available from Zillow(https://www.zillow.com/research/data/). Before estimating the densities, we divided all prices by \$1M and set the supports of $\{\mu_i\}_{i=1}^n$ and $\{\nu_i\}_{i=1}^n$ to be $[0, 1]$. We estimated the densities through kernel density estimation with bandwidth 0.1. For the Euclidean predictor, we obtained the FRED's 30-year fixed mortgage series MORTGAGE30US from Python package `pandas datareader`, a weekly national average commitment rate for conforming conventional purchase loans. Weekly values are averaged to monthly to align with our listing and sale price densities. The distributional responses and predictors, together with the corresponding Kantorovich potentials and optimal transport maps from the barycenter, as well as the Euclidean predictors, are visualized in Figure 7.

The fitted parameter $\widehat{f}'$ is shown in the left panel of Figure 8. We observe that $f'(t) \approx 1.2$ for $t \leq 0$, after which it decreases approximately linearly and falls below 1 once $t > 0.02$. Thus, the KR model amplifies displacements for small values of $\phi$ and attenuates them for larger values. When the listing price distribution lies to the right of $\bar{\mu}$, $\nabla\phi_{\bar{\mu}\to\mu} < 0$ and $\phi_{\bar{\mu}\to\mu}$ is decreasing. In this case, smaller values of $\phi$ correspond to the upper tail of the listing distribution (i.e., higher-priced homes). Since $f'(\phi)$ is larger in this region, the KR model

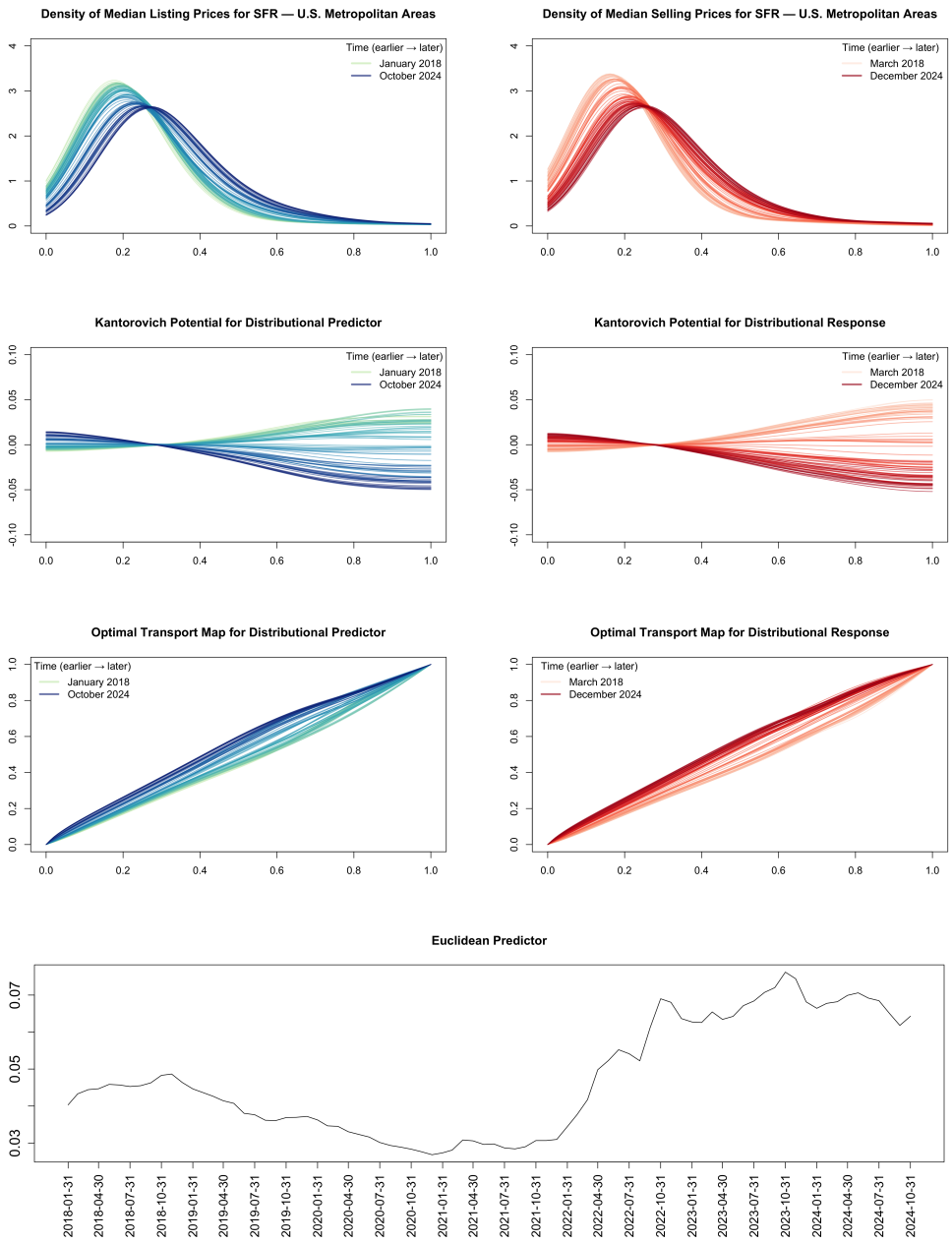


Figure 7: (Top left) Observed distributional predictor, (Top right) observed distributional response, (Upper left) observed Kantorovich potential for distributional predictor, (Upper right) observed Kantorovich potential for the distributional response, (Lower left) observed optimal transport map for distributional predictor, (Lower right) observed optimal transport map for the distributional response, and (Bottom) Euclidean Predictor.

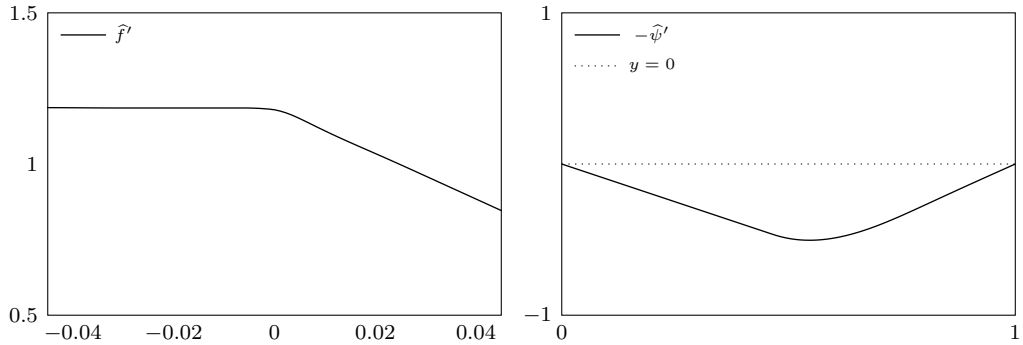


Figure 8: (Left) Estimated derivative $\widehat{f}'$ associated with the distributional predictor; (Right) Negative derivative $-\widehat{\psi}'$ of estimated functional parameter $\hat{\psi}$ associated with the Euclidean predictor $Z_i$.

amplifies the displacement from the barycenter in the upper tail of the sale distribution, while displacement in the lower tail is decreased. Conversely, when the listing distribution lies to the left of $\bar{\mu}$, $\nabla\phi_{\bar{\mu}\to\mu} > 0$ and $\phi_{\bar{\mu}\to\mu}$ is increasing. Smaller values of $\phi$ then correspond to the lower tail of the listing distribution (i.e., lower-priced homes). The KR model amplifies the displacement from the barycenter in the lower tail of the sale distribution, while displacement in the upper tail is attenuated. In economic languages, the model suggests that when the listing distribution lies to the right of the barycenter (i.e., the market is relatively strong or confident), the higher-price segment exhibits a larger deviation from the market barycenter in the sale distribution than in the listing distribution. Conversely, when the listing distribution lies to the left of the barycenter (i.e., the market is relatively weak), the lower-price segment exhibits a larger deviation.

On the other hand, the estimated functional parameter $\widehat{\psi}$ associated with the Euclidean predictor $X_i$, shown in the right panel of Figure 8, satisfies $-\widehat{\psi}'(x) \leq 0$ for any $x \in [0, 1]$. Recall that $-\psi'(x)$ represents the additional displacement between an individual distribution and the barycenter. Hence, the fact that $-\widehat{\psi}'(x)$ is uniformly negative indicates a leftward deformation that strengthens as $X_i$ increases. This pattern accords with market intuition: when mortgage rates are higher, sale-price distributions shift toward lower values.

In Figure 9, we predicted the March 2025 SFR sale-price density across U.S. metropolitan areas ($\nu_{\text{Mar,2025}}$) based on listing price density and the mortgage rate in January 2025, $\mu_{\text{Jan, 2025}}$ and $X_{\text{Jan, 2025}}$ through our model and estimated functional parameter $\widehat{f}$ and $\widehat{\psi}$. The

figure shows that the model rescales the predictor displacement to match the response displacement, especially on $[0, 0.7]$ where most of the masses of $\bar{\nu}$ is concentrated. As a result, the response density is predicted accurately, with the squared 2-Wasserstein distance between the observed and predicted March 2025 densities given by $\mathcal{W}_2^2\big(\nu_{\text{Mar 2025}}, \widehat{\nu}_{\text{Mar 2025}}\big) = 1.144 \times 10^{-5}$.

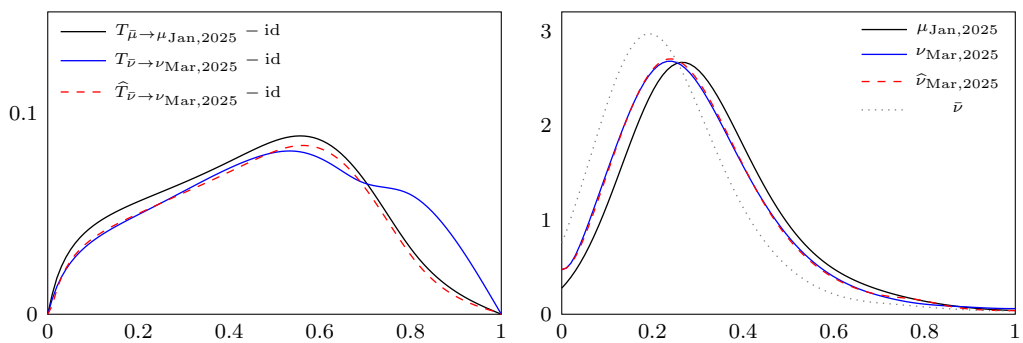


Figure 9: Prediction for the March 2025 SFR sale-price density across U.S. metropolitan areas. Left panel shows observed predictor displacement $T_{\bar{\mu}\to\mu_{\text{Jan,2025}}} - \text{id}$, response displacement $T_{\bar{\nu}\to\nu_{\text{Mar,2025}}} - \text{id}$ and predicted displacement $\widehat{T}_{\bar{\nu}\to\nu_{\text{Mar,2025}}} - \text{id}$. Right panel shows observed distributional predictor $\mu_{\text{Jan,2025}}$, observed distributional response $\nu_{\text{Mar, 2025}}$ and predicted response $\widehat{\nu}_{\text{Mar,2025}}$.

### 6.3. 2D real data

In this second real-data example, we demonstrate that Kantorovich regression can be applied to bivariate distributional predictors and responses. We use the joint distributions of daily minimum and maximum temperatures during the summer months (June–August) of 2000 and 2020, measured at 50 airports in the US. The daily minimum and maximum temperature data is available from https://www.ncdc.noaa.gov/cdo-web/datasets. We estimate the densities on the domain $[30, 100] \times [50, 120]$, where the first and second coordinates correspond to daily minimum and maximum temperatures, respectively, discretized on a $200 \times 200$ grid. The densities are obtained by smoothing two-dimensional histograms using a Gaussian filter. Using the bivariate distributions of daily minimum and maximum temperatures in summer 2000 as predictors, we aim to predict the corresponding temperature distributions in summer 2020 via model 4.

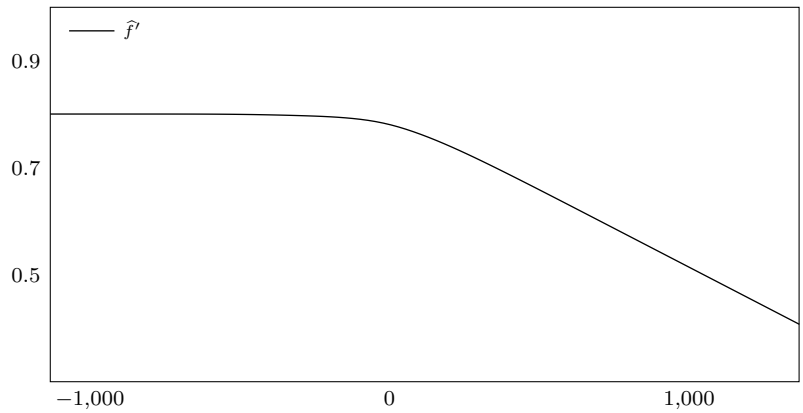


Figure 10: Estimated derivative $\widehat{f}'$ of the functional parameter $\widehat{f}$ for model 4.

We observe that the estimated functional parameter $\widehat{f}' < 1$. This indicates that the displacement vectors from the Wasserstein barycenter to each distribution have been contracted over the 20-year period, suggesting that the gap between summer temperature distributions across U.S. has decreased. A possible explanation is that colder regions have warmed faster than hotter regions, leading to a reduction in the regional discrepancies between summer daily temperature densities.

As shown in Figure 11, we did leave-one-out prediction for San Diego International Airport, CA and compared our result with geodesic optimal transport regression(GOT) [Zhu and Müller, 2025] on the Hilbert sphere and generalized Nadaraya-Watson regression estimator (GNW) [Steinke and Hein, 2008]. We observe that the location of the probability density predicted by our method is closest to that of the observed response density. Moreover, the displacement vector field is fitted to match both the direction and the magnitude of the response displacement vector through our model. The leave-one-out prediction errors of NW, GOT, and KR with respect to the squared 2-Wasserstein distance are 69.545, 119.422, and 11.544, respectively, highlighting the superiority of KR for regression between multivariate distributions in Wasserstein space.

## 7. Conclusion

The proposed Kantorovich regression framework can provide an intrinsic approach to modeling distributional responses in Wasserstein space. Unlike Euclidean spaces, Wasserstein

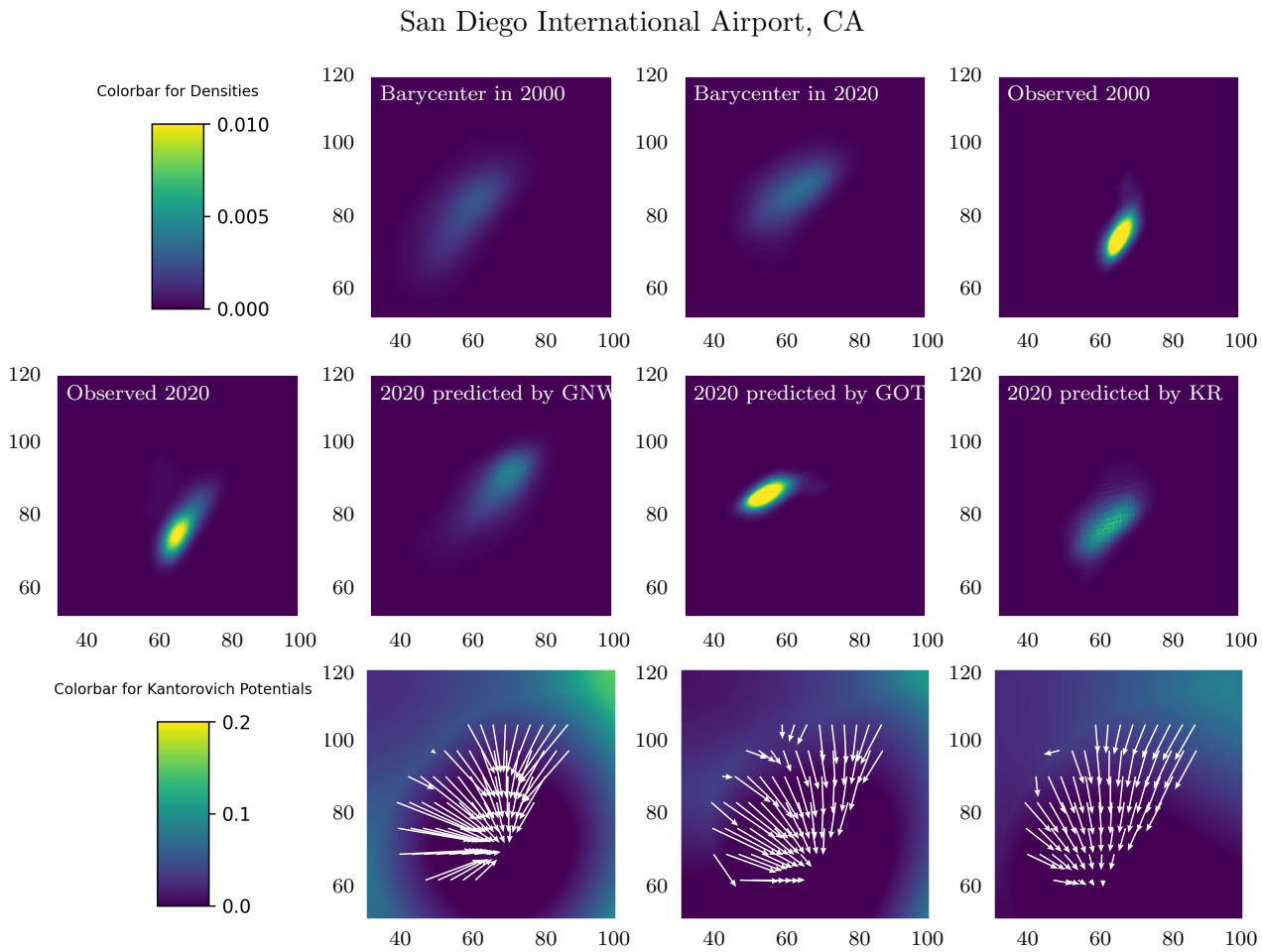


Figure 11: Illustration of leave-one-out prediction for the joint daily temperature density at San Diego International Airport, CA. Row 1: Wasserstein barycenter of the joint daily temperature densities (2000 in column 2, 2020 in column 3) and the observed joint daily temperature density in 2000 (column 4). Row 2: Observed joint daily temperature density in 2020 (column 1) and leave-one-out predictions for joint daily temperature density in 2020 obtained by GNW (column 2), GOT (column 3), and KR (column 4). Row 3: Kantorovich potential(heat map) and displacement vector(white arrow) for the observed predictor density (column 2), observed response density (column 3), and the density predicted by KR (column 4).

space is nonlinear, making classical regression formulations unsuitable. By leveraging the geometric structure of optimal transport, our method models covariate effects through displacement fields induced by Kantorovich potentials relative to the Wasserstein barycenter. In our model, displacement fields are scaled along the level sets of the corresponding Kantorovich potentials, allowing covariates to modulate the displacement field from the barycenter to the response distribution while respecting the intrinsic geometry of Wasserstein space. While much of the existing literature focuses on one-dimensional distributions, our framework naturally extends to multivariate distributions and, to the best of our knowledge, is the first regression framework in the optimal transport literature that accommodates mixed predictors consisting of both distributional and Euclidean variables.

## References


Agueh, M., & Carlier, G. (2011). Barycenters in the Wasserstein space. *SIAM J. Math. Anal.*, *43*(2), 904–924.

Amos, B., Xu, L., & Kolter, J. Z. (2017). Input convex neural networks. *Proceedings of the 34th International Conference on Machine Learning*, 146–155.

Berman, R. J. (2021). Convergence rates for discretized Monge–Ampère equations and quantitative stability of optimal transport. *Foundations of Computational Mathematics*, *21*(4), 1099–1140.

Bhatia, A., & Katz, J. (2021). Why we are experiencing so many unusually hot summer nights. *The New York Times*, *September 16*, A12.

Brenier, Y. (1991). Polar factorization and monotone rearrangement of vector-valued functions. *Communications on Pure and Applied Mathematics*, *44*(4), 375–417.

Carlier, G., Delalande, A., & Merigot, Q. (2024). Quantitative stability of barycenters in the wasserstein space. *Probability Theory and Related Fields*, *188*(3), 1257–1286.

Chen, X., Fu, M., Huang, Y., & Deng, X. (2024). Distribution-in-distribution-out regression. *arXiv preprint arXiv:2405.11626*.

Chen, Y., Lin, Z., & Müller, H.-G. (2023). Wasserstein regression. *Journal of the American Statistical Association*, *118*(542), 869–882.

Chen, Y., Li, T., Bai, Y., & Lin, Z. (2026). Multi-transport distributional regression. *arXiv preprint arXiv:2601.03674*.

Chewi, S., Niles-Weed, J., & Rigollet, P. (2025). *Statistical optimal transport*. Springer.

Divol, V., Niles-Weed, J., & Pooladian, A.-A. (2025). Optimal transport map estimation in general function spaces. *The Annals of Statistics*, *53*(3), 963–988.

Ghodrati, L., & Panaretos, V. M. (2022). Distribution-on-distribution regression via optimal transport maps. *Biometrika*, *109*(4), 957–974.

Ghodrati, L., & Panaretos, V. M. (2024). On distributional autoregression and iterated transportation. *Journal of Time Series Analysis*, *45*(5), 739–770.

Girshfeld, I., & Chen, X. (2025). Neural local wasserstein regression. *Conference on Topology, Algebra, and Geometry in Data Science (TAG-DS)*.

Hütter, J.-C., & Rigollet, P. (2021). Minimax estimation of smooth optimal transport maps. *The Annals of Statistics*, *49*(2), 1166–1194.

Jacobs, M., Lee, W., & Léger, F. (2021). The back-and-forth method for wasserstein gradient flows. *ESAIM: Control, Optimisation and Calculus of Variations*, *27*, 28.

Jdanov, D., Jasilionis, D., Shkolnikov, V., & Barbieri, M. (2021). Human mortality database. In *Encyclopedia of gerontology and population aging* (pp. 2495–2503). Springer International Publishing.

Kim, K., Yao, R., Zhu, C., & Chen, X. (2025). Optimal transport barycenter via nonconvex concave minimax optimization. *Proceedings of the International Conference on Machine Learning*.

Kim, K., Zhou, B., Zhu, C., & Chen, X. (2026). Sobolev gradient ascent for optimal transport: Barycenter optimization and convergence analysis. *International Conference on Learning Representations (ICLR)*.

Kokoszka, P., Miao, H., Petersen, A., & Shang, H. L. (2019). Forecasting of density functions with an application to cross-sectional and intraday returns. *International Journal of Forecasting*, *35*(4), 1304–1317.

Le Gouic, T., Paris, Q., Rigollet, P., & Stromme, A. J. (2022). Fast convergence of empirical barycenters in alexandrov spaces and the wasserstein space. *Journal of the European Mathematical Society*, *25*(6), 2229–2250.

Manole, T., Balakrishnan, S., Niles-Weed, J., & Wasserman, L. (2024). Plugin estimation of smooth optimal transport maps. *The Annals of Statistics*, *52*(3), 966–998.

Matabuena, M., & Petersen, A. (2023). Distributional data analysis of accelerometer data from the nhanes database using nonparametric survey regression models. *Journal of the Royal Statistical Society Series C: Applied Statistics*, *72*(2), 294–313.

Panaretos, V. M., & Zemel, Y. (2016). Amplitude and phase variation of point processes. *The Annals of Statistics*, *44*(2), 771–812.

Panaretos, V. M., & Zemel, Y. (2020). *An invitation to statistics in wasserstein space*. Springer New York.

Paty, F.-P., d'Aspremont, A., & Cuturi, M. (2020). Regularity as regularization: Smooth and strongly convex brenier potentials in optimal transport. *International Conference on Artificial Intelligence and Statistics*, 1222–1232.

Petersen, A., & Müller, H.-G. (2016). Functional data analysis for density functions by transformation to a Hilbert space. *44*(1), 183–218.

Petersen, A., & Müller, H.-G. (2019). Wasserstein covariance for multiple random densities. *Biometrika*, *106*(2), 339–351.

Rockafellar, R. (1966). Characterization of the subdifferentials of convex functions. *Pacific Journal of Mathematics*, *17*(3), 497–510.

Santambrogio, F. (2015). *Optimal transport for applied mathematicians*. Birkhäuser.

Steinke, F., & Hein, M. (2008). Non-parametric regression between manifolds. *Advances in Neural Information Processing Systems*, *21*.

Van der Vaart, A., & Wellner, J. (2023). *Weak Convergence and Empirical Processes* (2nd). Springer, New York.

Zhang, Z., & Müller, H.-G. (2011). Functional density synchronization. *Computational Statistics & Data Analysis*, *55*(7), 2234–2249.

Zhu, C., & Müller, H.-G. (2023). Autoregressive optimal transport models. *Journal of the Royal Statistical Society Series B: Statistical Methodology*, *85*(3), 1012–1033.

Zhu, C., & Müller, H.-G. (2025). Geodesic optimal transport regression. *Biometrika*, in press.